

This dissertation has been
microfilmed exactly as received 66-14,192

ANDERSON, Richard John, 1938-
EXCITATION OF MERCURY ATOMS BY
ELECTRON IMPACT.

The University of Oklahoma, Ph.D., 1966
Physics, spectroscopy

University Microfilms, Inc., Ann Arbor, Michigan

THE UNIVERSITY OF OKLAHOMA

GRADUATE COLLEGE

EXCITATION OF MERCURY ATOMS BY ELECTRON IMPACT

A DISSERTATION

SUBMITTED TO THE GRADUATE FACULTY

in partial fulfillment of the requirements for the

degree of

DOCTOR OF PHILOSOPHY

BY

RICHARD JOHN ANDERSON

Norman, Oklahoma

EXCITATION OF MERCURY ATOMS BY ELECTRON IMPACT

APPROVED BY

Chun C. Lin

S. E. Bobb, Jr.

Robert M. St. John

Earl L. Gorn

Jim Confield

DISSERTATION COMMITTEE

ACKNOWLEDGMENTS

The author wishes to express his sincere appreciation to Dr. Chun C. Lin for suggesting the research problem and for his guidance during the course of the investigation.

It is also a pleasure to acknowledge Dr. S. B. J. Corrigan and Dr. R. M. St. John for their helpful discussions concerning the experimental aspects of this paper.

In addition sincere thanks are extended to Rev. N. Alexandre, R. L. Legan, J. A. Payne, and F. A. Sharpton for their help in the design and construction of the experimental apparatus. Special acknowledgment is accorded to E. T. P. Lee, for his invaluable work on the theoretical aspects of this paper.

Finally, a warm thank you is extended to my wife Susan, for relinquishing her marital right of companionship, to my experimental apparatus, during the duration of the investigation.

TABLE OF CONTENTS

	Page
LIST OF TABLES.....	vi
LIST OF ILLUSTRATIONS.....	vii
CHAPTER	
I. INTRODUCTION.....	1
Theory	
II. MERCURY STRUCTURE.....	7
Spin-Orbit Perturbation	
Transition Probabilities	
III. RELATIVE MEASUREMENTS.....	19
Experimental Apparatus	
Optical Excitation Functions	
Triplet S and P Levels	
Singlet S and P Levels	
D Levels	
Comparison With Other Investigators	

Table of Contents Continued

	Page
IV. ABSOLUTE MEASUREMENTS.....	60
Experimental Procedure	
Effective Excitation Cross Sections	
Comparison With Other Investigators	
Intensity Ratios of Lines Originating from a Common Upper Level	
V. CASCADE ANALYSIS.....	84
Direct Excitation Cross Section; 6^3D_3 Level	
Direct Excitation Cross Section; 6^3D_2 Level	
Direct Excitation Cross Section; 7^3P_2 Level	
Direct Excitation Cross Section; 7^1S Level	
Comparison With Theory	
VI. CONCLUSIONS.....	99
LIST OF REFERENCES.....	103

LIST OF TABLES

Table	Page
I. Energy Matrix in the Coupled Representation.....	10
II. Spontaneous Transition Probabilities.....	18
III. Effective Excitation Cross Sections $n^1P - 7^1S$	66
IV. Effective Excitation Cross Sections $n^1P - 7^3S$	67
V. Effective Excitation Cross Sections $n^3P - 7^3S$	68
VI. Effective Excitation Cross Sections $nS - 6^1P$	70
VII. Effective Excitation Cross Sections $nD - 6^1P$	71
VIII. Effective Excitation Cross Sections $nD - 6^3P_2; n^1S - 6^3P_1$	72
IX. Comparison of Effective Excitation Cross Sections.....	74
X. Intensity Ratios of the Visible Mercury Triplet.....	80
XI. Intensity Ratios of Lines Originating from the 7^1S and n^1P Levels.	83
XII. Comparison of Experimental and Theoretical Direct Excitation Cross Sections.....	98

LIST OF ILLUSTRATIONS

Figure	Page
1. Experimental Apparatus.....	21
2. Electron Gun.....	22
3. Electron Beam Current Regulator.....	24
4. Integrating Amplifier.....	27
5. Tuned Amplifier.....	28
6. Phase Sensitive Detector.....	29
7. Control Experiments; $8^1P - 7^1S$ (50 eV).....	32
8. Control Experiments; $7^3S - 6^3P_{2,1,0}$ (50 eV).....	33
9. Optical Excitation Functions; $n^3P - 7^3S$ (0 - 90 eV).....	36
10. Optical Excitation Functions; $n^3P - 7^3S$ (0 - 90 eV).....	37
11. Optical Excitation Functions; $nS - 6P$ (0 - 90 eV).....	40
12. Optical Excitation Functions; $n^1P - 7^3S$ (0 - 90 eV).....	42
13. Optical Excitation Functions; $n^1P - 7^1S$ (0 - 90 eV).....	43
14. Optical Excitation Functions; $nD - 6P$ (0 - 90 eV).....	48
15. Optical Excitation Functions for the Transitions of Primary Interest (0 - 90 eV).....	49

List of Illustrations Continued

Figure		Page
16.	Optical Excitation Function; $7^3S - 6^3P_2$ (0 - 18 eV).....	51

THE EXCITATION OF MERCURY BY ELECTRON IMPACT

CHAPTER I

INTRODUCTION

Recent advances in the physics of the upper atmosphere and laser technology have promoted a renewed interest in the study of collision phenomena. Technological improvements in photomultipliers and allied electronic detection apparatus have made possible rapid and accurate measurements of collision parameters. The study of the excitation of mercury by electron impact provides useful information concerning the collision properties of a two-valence electron, heavy atom. This knowledge is of special interest since the states of the mercury atom experience nonvanishing coupling between L and S and hence are not pure states, but instead are singlet-triplet mixtures. Because of this mixture property the quantum number S is no longer valid and intense intercombination transitions may occur. In addition the 6D states experience an inversion of the singlet and triplet energy levels which may be ascribed to the effects of configuration interaction.

Because of these properties and many others (e.g. availability, spectral range, etc) mercury has been the subject of intensive study. Since 1928 numerous investigators ⁽¹⁻⁵⁾ have studied the excitation processes involving electron-atom collisions in mercury. Relative and absolute measurements have been carried out describing the intensity of spectral emission as a function of the energy of the incident electron. The most recent of the absolute measurements are those of H. M. Jongerius ⁽⁶⁾ for transitions in the wavelength range 248.5 nm to 579.1 nm. The present work has yielded relative and absolute measurements of the emission cross section for 45 spectral transitions in the wavelength interval 365.0 nm to 1128.7 nm. Theoretical calculations have been employed to determine the spontaneous transition probabilities for several transitions. These values enable one to calculate the probability of excitation to a particular excited level, which results from a ground state atom experiencing an electron collision. Such probabilities, or direct excitation cross sections, were calculated for the 7^1S , 7^3P_2 , 6^3D_2 , and 6^3D_3 levels of mercury at an incident electron energy of 15 eV. The values obtained in this manner are compared to the theoretical calculations made by E. T. P. Lee ⁽⁷⁾, using the Born and Born-Oppenheimer approximations. The theoretical transition probabilities are also used to determine the intensity ratios of spectral lines emanating from a common upper level. The calculated ratios are compared to those obtained experimentally and observations are made regarding their agreement.

Theory

An electron traveling through mercury vapor experiences collisions with the constituent atoms. The collisions can be classified as being inelastic or elastic, dependent upon whether or not a significant quantity of energy is transferred to the internal motion of the neutral atom. Inelastic collisions are further divided into four sub-cases; ionization, single excitation, double excitation, and ionization-excitation. This work will deal exclusively with the single excitation process.

The excitation process is described by employing the concept of cross section, which is proportional to the probability of excitation. The number density of neutral atoms excited to the j th state by electron impact is given as

$$\delta N(j) = N(g)(I/eS)Q(j) , \quad (1)$$

where $N(g)$ is the number density of ground state atoms, (I/eS) is the electron flux, and $Q(j)$ is the direct excitation cross section for the j th level. The variation of the excitation cross section as a function of incident electron energy is called an electronic excitation function. This is usually obtained by observing the loss of kinetic energy of the incident electrons to the internal motion of the neutral atoms. The relation between the number of electrons, which lose an amount of kinetic energy equal to that of the j th level, and the energy of the incident electrons determines the functional dependence. The

collision process can also be investigated by observing the radiation emitted as the excited atoms return to states of lower energy. The functional relation between the intensity of a spectral line and the incident electron energy is called the optical excitation function. The two types of excitation functions differ significantly because the excited level can be populated by additional mechanisms. In addition to direct population by electron impact, the j th excited level experiences a gain in population through radiative transitions from upper levels (cascade gain), and nonradiative collisions of excited atoms with electrons, neutral atoms, and other excited atoms, (superelastic collisions). The level also experiences a population decrease through radiative transitions to lower levels and through superelastic collisions such as those previously described. The optical excitation function will consist of the sum of the electronic excitation function of the j th level and the excitation functions representing the levels which contribute to its population by cascade transitions. The influence of superelastic collisions is made negligible by carrying out the experimental investigation under conditions of low electron and atom densities, thus insuring a single electron-atom collision process.

The steady state population equation for the j th excited level, under the assumption of single atom-electron collision processes, is given as

$$\text{Cascade loss} = \text{Electron impact gain} + \text{Cascade gain}.$$

The gain of population through electron impact is proportional to the direct

excitation cross section, therefore the direct cross section can be expressed in terms of the cascade contributions to and from the j th level. It is experimentally possible to determine the number of photons per cm of electron beam emitted in a particular radiative transition from the j th level to a lower level. Hence, it is common experimental practice to define an effective excitation cross section, in terms of these determinable quantities, as

$$Q(j,k) = \frac{J(j,k)}{(I/e) N(g)} , \quad (2)$$

where $J(j,k)$ is the number of photons emitted per cm of electron beam in the $j \rightarrow k$ transition, and the definitions of I/e and $N(g)$ remain unchanged from the previous case. One can also consider the apparent excitation cross section for the j th level which is the sum of the direct cross section and the cascade contributions from higher levels. The apparent excitation cross section is proportional to the effective excitation cross section and is defined by the relation

$$Q'(j) = Q(j,k)B(j,k) , \quad (3)$$

where $B(j,k)$ is the theoretical branching ratio. The branching ratio is simply the ratio of the total transition probability, for radiative transitions from the j th level to all lower levels, to the transition probability of a radiative transition from the j th to k th levels.

The collision process is described by three quantities, which

correspond to different steps of the analysis. The initial experimental measurements yield effective excitation cross sections which are proportional to the intensities of the observed radiative transitions. These are converted into apparent excitation cross sections by multiplication with the theoretical branching ratio. The apparent excitation cross section better describes the electron-atom collision process, but it is not corrected for the effects of cascade transitions. Subtraction of the cascade contribution from the apparent cross section results in the formation of the direct excitation cross section. The latter quantity describes the effectiveness with which the j th excited level is populated by collisions of electrons with ground state atoms. The direct cross section is of prime importance and the efforts of this work will be directed to evaluating this quantity for various excited states of mercury.

CHAPTER II

MERCURY STRUCTURE

Mercury, with an atomic number of 80 and two valence electrons, (corresponding to a ground state term 6^1S), has a spectrum characterized by intense intercombination transitions. The transitions, which violate the $\Delta S = 0$ selection rule of pure L-S coupling, arise because the rule is valid only under the assumption of vanishing spin-orbit interaction. Atoms with large atomic numbers experience a non-vanishing coupling between their spin and orbital angular moments, resulting in levels which possess both singlet and triplet components. The degree of deviation from the pure L-S scheme is indicated by the magnitude of the singlet-triplet mixing coefficients, which describe the state. A detailed analysis of the problem will be carried out in the following section and the resulting wave functions will be used to calculate the transition probabilities of several states.

Singlet-Triplet Mixtures

One studies the effects of singlet-triplet mixing by treating the

spin-orbit interaction energy as a perturbation to the non-relativistic hamiltonian of the atom. In this analysis one adopts the usual approximation that, the influence of spin-other orbit interactions will be negligible, when compared to that of the spin-self orbit interaction. Therefore the resulting hamiltonian is given as $H = H_0 + H_1$, where

$$H_0 = \sum_{\text{electrons}} \frac{p^2}{2m} - Ze^2/r + \sum_{\text{pairs}} e^2/r_{12}, \quad (4)$$

and

$$H_1 = \sum_{\text{electrons}} \zeta(r) \underline{L} \cdot \underline{S}. \quad (5)$$

One chooses a representation in which H_0 is diagonal and then diagonalizes the energy matrix to obtain the eigenvalues and eigenfunctions which describe the perturbed state. H_0 commutes with L, S, J , and M , therefore the energy matrix is set up in the coupled representation. The basis functions for this representation are obtained in the following manner. As an initial step the wave functions in the decoupled representation,

$$\Phi (LSM_L M_S) = \phi (LM_L) \chi (SM_S) \quad (6)$$

are obtained by forming the anti-symmetric product of the spin and orbital wave functions for the $(6s)(n\ell)$ configuration. The resulting wave functions are then mixed by means of Clebsch-Gordan coefficients to yield the wave function in the coupled representation,

$$\Psi(\text{LSJM}) = \sum_{M_L, M_S} |C_{M_L M_S M}^{\text{LSJ}}|^2 \Phi(\text{LSM}_L M_S). \quad (7)$$

The resultant functions are used to set up the energy matrix for the $(6s)(n\ell)$ configuration, which yields the terms $3_{L_{\ell+1}}$, $3_{L_{\ell}}$, $1_{L_{\ell}}$, and $3_{L_{\ell-1}}$. It is well known that the energy is independent of the value of M_L and M_S , therefore since the LSJM state is a linear combination of the $\text{LSM}_L M_S$ states, with different M_L, M_S , but the same values of L and S , the energy will be independent of the value of M . Hence, one need only to evaluate the terms for the largest value of M for which all of the states exist.

The energy matrix, displayed in Table I, has non-diagonal elements connecting the $3_{L_{\ell}}$ and $1_{L_{\ell}}$ states. Thus in order to obtain the eigenfunctions and eigenvalues corresponding to these levels, one must solve a 2×2 secular determinant. The eigenvalues of the secular equation will correspond to the energies associated with the perturbed levels, hence the resultant energy levels are given as

$$E_1 = E(3_{L_{\ell+1}}) = A - K - \frac{1}{2} \ell \rho_{n\ell} \quad (8)$$

$$E_2 = E(3_{L_{\ell}}) = A - \frac{1}{4} \rho_{n\ell} + \sqrt{\left(K + \frac{1}{4} \rho_{n\ell}\right)^2 + \frac{1}{4} \ell(\ell+1) \rho_{n\ell}^2} \quad (9)$$

$$E_3 = E(1_{L_{\ell}}) = A - \frac{1}{4} \rho_{n\ell} - \sqrt{\left(K + \frac{1}{4} \rho_{n\ell}\right)^2 + \frac{1}{4} \ell(\ell+1) \rho_{n\ell}^2} \quad (10)$$

$$E_4 = E(3_{L_{\ell-1}}) = A - K - \frac{1}{2} (\ell+1) \rho_{n\ell}. \quad (11)$$

TABLE I
ENERGY MATRIX IN THE COUPLED REPRESENTATION

A is a constant whose magnitude is equal to the sum of the $(6s)(n\ell)$ configuration energy and the corresponding coulomb energy, K is the $(6s)(n\ell)$ exchange integral, and $\rho_{n\ell}$ is a radial integral involving the spin orbit coupling constant.

	$3L_{\ell+1}$	$3L_{\ell}$	$1L_{\ell}$	$3L_{\ell-1}$
$3L_{\ell+1}$	$A - K + \frac{1}{2} \rho_{n\ell}$			
$3L_{\ell}$		$A - K - \frac{1}{2} \rho_{n\ell}$	$\frac{\sqrt{\ell(\ell+1)}}{2} \rho_{n\ell}$	
$1L_{\ell}$		$\frac{\sqrt{\ell(\ell+1)}}{2} \rho_{n\ell}$	$A + K$	
$3L_{\ell-1}$				$A - K - \frac{(\ell+1)}{2} \rho_{n\ell}$

The eigenvectors corresponding to $E(3_{L\ell})$ and $E(1_{L\ell})$ are evaluated and are placed side by side to yield the inverse of the transformation matrix, which diagonalizes the 2×2 block. The elements of the transformation matrix are the coefficients used in forming the perturbed eigenfunction as a linear combination of the unperturbed functions. The perturbed eigenfunctions

$$\Psi'(3_{L\ell}) = a\Psi(3_{L\ell}) + b\Psi(1_{L\ell}), \quad (12)$$

and

$$\Psi''(1_{L\ell}) = -b\Psi(3_{L\ell}) + a\Psi(1_{L\ell}) \quad (13)$$

are a mixture of the singlet and triplet states. The degree of mixing is indicated by the value of the mixing coefficients a , and b which are defined through the relations

$$a = \frac{\sqrt{(p^2 + q^2)} + q}{N}, \quad b = \frac{p}{N}, \quad (14)$$

where

$$p = \frac{1}{2} \rho_{n\ell} \sqrt{(\ell+1)}, \quad q = \frac{1}{4} \rho_{n\ell} + K \quad (15)$$

and

$$N = \sqrt{(\sqrt{p^2 + q^2} + q)^2 + p^2}. \quad (16)$$

The magnitude of the mixing coefficients can be obtained by employing empirically determined values of the term energies ⁽⁸⁾, and solving the resulting equations, (c.f. eqs. 8-11) for the parameters, K and $\rho_{n\ell}$, which are used in their determination. One notes immediately that the coefficients are over determined since four equations define three unknown quantities, $\rho_{n\ell}$, K , and A . One must solve the equations so that the three parameters assume the best possible fit with respect to the experimental energy levels, and then place a range on the acceptable fitted values.

For instance in the case of the $(6s)(6p)$ configuration this analysis yielded a "best fit" value of $b = 0.20$. On the other hand, if $\rho_{n\ell}$ is determined exactly in terms of one of the energy spacings and K is determined from the remaining two energy differences, then the coefficient assumes the value $b = 0.120$. One can estimate a range of acceptable values by determining the values of K and $\rho_{n\ell}$, (and ultimately that of b), for which the percentage difference between the calculated and experimental values of the energy levels exceed a reasonable limit. In this manner the range of acceptable values for the $(6s)(6p)$ mixing coefficient lies within the values $b = 0.120$ and $b = 0.210$. This estimate leads to a mean value of $b = 0.165 \pm 0.045$. One can apply a similar analysis to the $(6s)(7p)$ configuration. In this case the "best fit" value of the mixing coefficient was determined as $b = 0.52$. One also estimates the range of acceptable values as that which lies within the values $b = 0.46$ and $b = 0.62$. The ambiguity (or range), present in the magnitude

of the mixing coefficient results from the approximate nature of the theory. The magnitude of the range gives one an estimate of the accuracy of the theoretical model, which in the present analysis is a single configuration approximation.

Alternately one can determine the magnitude of the mixing coefficient from the experimental g-factor. In this procedure the magnitude of the mixing coefficient is given directly by one experimental number. This eliminates the need for a "best fit" analysis, which ultimately introduces a range into the magnitude of the coefficient. The elimination of a range of acceptable values also eliminates a means by which one can check the self consistency of the theory. A. Lurio ⁽⁹⁾ and R. I. Semenov ⁽¹⁰⁾ have determined the value of the (6s)(6p) mixing coefficient from experimental g factors. Their reported values are $b = 0.1725$ and $b = 0.180$ respectively. Lurio also determined the mixing coefficient by means of fine structure analysis (two parameter theory) and from lifetime measurements. The fine structure analysis yielded a value of $b = 0.1582$ while a value of $b = 0.1714$ resulted from the investigation of lifetimes. The various methods yield values which exhibit good agreement. In addition, all of these values lie within the range of acceptable values predicted by the fine structure analysis. Therefore the forthcoming analysis will employ a mean value of the (6s)(6p) and (6s)(7p) mixing coefficients, which takes into consideration the values obtained from the various methods. The mean value of the (6s)(6p) mixing coefficient is determined as $b = 0.165 \pm 0.045$, where the range is that determined from the fine structure analysis.

The D states are in contradiction to the theory outlined above, in that experimental observation shows that the $1D$ levels lie below the $3D$ levels on an energy scale. This discrepancy could be due to the neglect of configuration interaction and spin-other orbit interaction in the present approximation. Wolfe⁽¹¹⁾ has introduced the spin-other orbit interaction, as a fourth parameter, into the theoretical expression. In principle, one can use Wolfe's formula to obtain a unique determination of b . A major drawback of this approach is that it does not clearly illustrate that the spin-other orbit interaction, which is presumably small, is of sufficient magnitude to account for the "anomalous inversion" of the $1D$ and $3D$ states. One may be just introducing more parameters to fit the experimental results, without adequate justification. As an alternative approach one computes the value of b by employing both the g -factor and Wolfe's formula, and then examines the variation of these values to obtain the final selected value. Wolfe's formula yields a value $b = 0.557$ for the $(6s)(6d)$ mixing coefficient, while the experimental g -factor reported by Th. A. M. Van Kleeef⁽¹²⁾ yields a value of 0.575 ± 0.01 . The selected value corresponds to that reported by Semenov, and has the magnitude $b = 0.568 \pm 0.017$, which has a range that includes both of the previous values.

Transition Probabilities

For an atom in an excited level A there exists a definite probability, per unit time, of experiencing a spontaneous transition, with the emission

of radiation, to a lower level B. The transition probability is defined, in the usual manner as

$$A(A, B) = \frac{64\pi^4 \sigma^3}{3h} \frac{S(A, B)}{2J_A + 1} \quad (17)$$

where σ is the energy difference between A and B expressed in cm^{-1} , h is Planck's constant, $S(A, B)$ is the line strength of the transition, and J_A is the total angular momentum of the upper level. The line strength can be expressed as a sum over the components a, b of the dipole matrix element, such that

$$S(A, B) = \sum_{a, b} | \langle a | \underline{P} | b \rangle |^2. \quad (18)$$

The wave functions obtained in the previous section are employed in the calculation of the line strengths for the $(6s)(n\ell) \rightarrow (6s)(n'\ell')$ transitions.

The strength of the line for the transition $(6s)(n\ell) \rightarrow (6s)(n'\ell')$ is given as

$$S(\alpha j m; \alpha' j' m') = \sum_{m, m'} | \langle \alpha j m | \underline{P} | \alpha' j' m' \rangle |^2 \quad (19)$$

where non-vanishing matrix elements exist only if m changes by -1 or 0 . The formulae of Condon and Shortley ⁽¹³⁾ are used to evaluate the matrix elements, with the observation that the sum over m (from $m = -j$ to $m = +j$) of the submatrix elements, merely introduces a factor of $2J_A + 1$ since it is independent of m . The expression for the line strength becomes

$$S(\alpha j; \alpha' j') = (2J_A + 1) |(\alpha j | P | \alpha' j')|^2 Z(j, j'), \quad (20)$$

where

$$Z(j, j+1) = (j+1)(2j+3); \quad Z(j, j) = j(j+1); \quad Z(j, j-1) = j(2j-1).$$

The submatrix element can be evaluated by using the formulae of Condon and Shortley and the assignment $j_1 \equiv S$, $j_2 \equiv L$, $j \equiv J$. This procedure yields the expression

$$|(\alpha j | P | \alpha' j')|^2 = G(LSJ) |(\gamma l_2 | P | \gamma' l_2')|^2, \quad (21)$$

which contains a one electron submatrix element. The element is readily evaluated as

$$|(\gamma l_2 | P | \gamma' l_2')|^2 = g(l_2) |P(n l_2) - P(n' l_2')|^2. \quad (22)$$

The quantities G and g , which appear in the above expressions, are functions of the quantum numbers and are determined by the recursion formulae of Condon and Shortley.

The values of the radial integrals were obtained from a calculation by Mishra ⁽¹⁴⁾, which employed the S.C.F. wave functions of mercury.

The line strengths involving singlet-triplet intercombination transitions, (heretofore prohibited), will have non-zero values, which are proportional to the strengths of the corresponding allowed transitions. The constant of proportionality will be the ratio of the squares of the singlet-triplet mixing

coefficients, e.g.

$$S(3L_{\ell}, 1L_{\ell}) = \frac{b^2}{a^2} S(1L_{\ell}, 1L_{\ell}). \quad (23)$$

The transition probabilities corresponding to the transitions of primary importance in the cascade analysis are listed in Table II. The values of the $(6s)(7s) \rightarrow (6s)(6p)$ transition probabilities were obtained using the medium value of the mixing coefficients obtained in the previous section, while those corresponding to the $(6s)(6d) \rightarrow (6s)(6p)$ transitions employed the coefficients reported by Semenov. In addition probabilities for the $(6s)(7p) \rightarrow (6s)(7s)$ transitions were calculated using the mixing coefficients obtained from fine structure considerations.

The values of Table II are used to obtain the theoretical branching ratios for particular spectral transitions. The branching ratio is defined as the ratio of the total probability for a transition from the j th state to all lower states to the probability of a transition from the j th to the k th state, i.e.

$$B(j, k) = \frac{\sum_{i < j} A(i, j)}{A(j, k)}. \quad (24)$$

The magnitude of the branching ratio describes the efficiency with which the j th excited upper state redistributes its population to the k th state through radiative transitions. Knowledge of the branching ratio is a prerequisite for a meaningful analysis of the radiation produced in collision processes.

TABLE II

SPONTANEOUS TRANSITION PROBABILITIES

Transition	$A(i,k)$ (10^8 sec^{-1})	Transition	$A(i,k)$ (10^8 sec^{-1})	Transition	$A(i,k)$ (10^8 sec^{-1})
$7^3S-6^3P_2$	1.1	$6^3D_2-6^3P_2$	0.54 ± 0.02	$7^3P_2-7^3S$	0.44
$7^3S-6^3P_1$	1.2	$6^3D_2-6^3P_1$	3.3 ± 0.02	$7^3P_1-7^3S$	0.18
$7^3S-6^3P_0$	0.52	$6^3D_2-6^1P$	0.16 ± 0.04	$7^3P_0-7^3S$	0.23
7^3S-6^1P	0.002 ± 0.001			$7^3P_1-7^1S$	0.043 ± 0.008
7^1S-6^1P	0.29			7^1P-7^1S	0.18
$7^1S-6^3P_1$	0.13 ± 0.07			7^1P-7^3S	0.15 ± 0.03
				$7^3P_1-6^1S$	0.12 ± 0.03
				7^1P-6^1S	0.37

Note: The transition probabilities for the $7^3S-6^3P_{2,1,0}$ transitions are insensitive to changes in the magnitude of the mixing coefficient.

CHAPTER III

RELATIVE MEASUREMENTS

Experimental Apparatus

The experimental apparatus used in the investigation consists of three components: (1) a vacuum system and source of mercury atoms, (2) an electron gun to provide a constant flux of electrons into a field free collision zone, and (3) auxiliary equipment to detect and record the collisional radiation.

The vacuum system was constructed of glass and evacuated by means of an adequately trapped oil diffusion pump and mechanical forepump. The vacuum chamber was initially evacuated to a pressure of 2×10^{-7} Torr and was sealed off during the measurements. During this time the residual gas pressure was estimated to be less than 5×10^{-5} Torr, therefore the effect of superelastic collisions involving impurity atoms was negligible. The number density of mercury atoms was determined by regulating the temperature of a mercury droplet situated in an appendage to the chamber. The relation

between the temperature of the droplet and its saturated vapour pressure was obtained from the values of the Ernsberger and Pitman.⁽¹⁵⁾ The number density of the atoms is obtained by assuming that, for the temperature range 12°C to 30°C, the mercury vapour behaves as an ideal gas. A block diagram of the experimental apparatus is displayed in Fig. 1.

The mercury atoms are excited by a beam of univelocity electrons directed into a field free collision chamber. The beam is produced by an electron gun of pentode design displayed in Fig. 2. An indirectly heated oxide coated cathode provides a source of electrons, which are accelerated and collimated by focusing grids acting as a pin hole electron lens. The collimated beam passes into a cylindrical faraday cup, bounded at its rear by a metal screen. A second smaller cylinder which acts as an electron collector, is situated to the rear of the screen and is concentric to the faraday cup. The collector is operated at a positive voltage, with respect to the chamber, in order to minimize the effects of secondary and reflected electrons. A small window in the side of the faraday cup allows the radiation to be observed at right angles to the electron beam.

Although the energy of the incident electrons is continuously varied by a programmed D.C. power supply, the electron beam current into the collision chamber is held constant by a degenerative feed back system. The system samples the chamber current by monitoring the voltage developed across a small resistor, placed in the return path from the collision chamber-

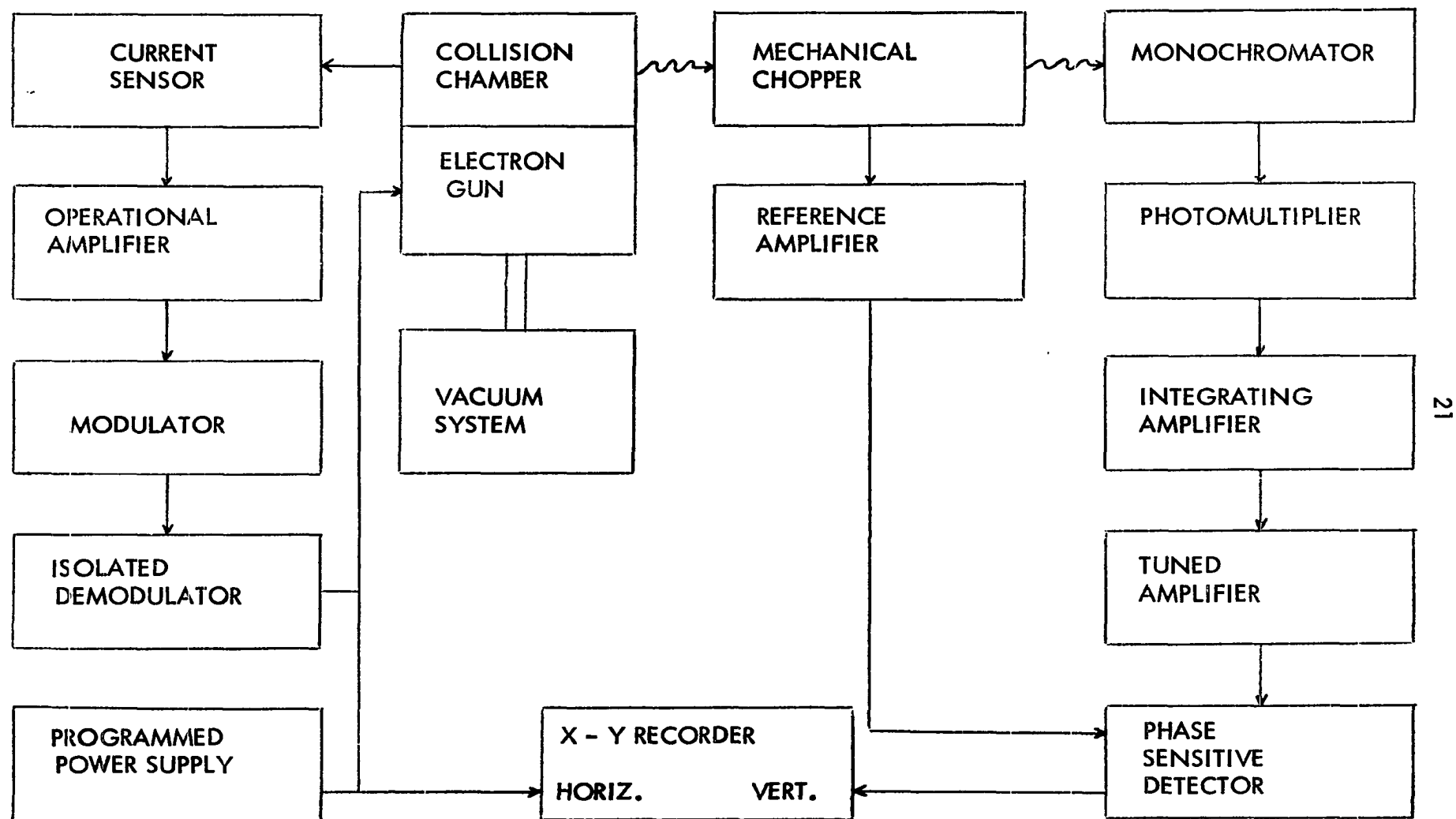


FIGURE 1. EXPERIMENTAL APPARATUS

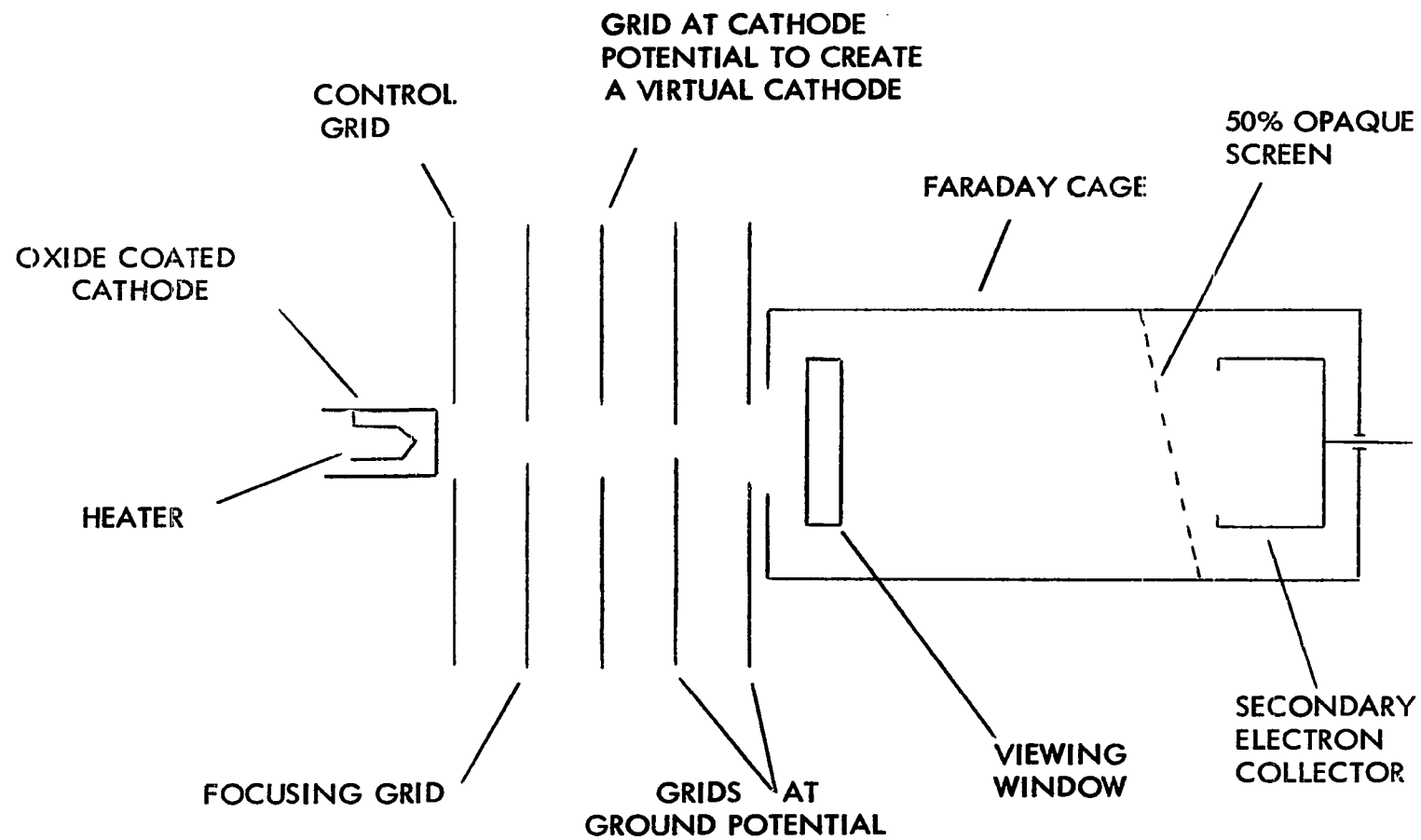


FIGURE 2. ELECTRON GUN

collector system. The feed back system remains passive until the beam current exceeds a pre-determined level, at which time an electronic comparator converts the difference between the actual and the desired current values into a voltage signal. This signal is amplified by a chopper stabilized D.C. amplifier, which is operated with negative feedback to insure its stability. The output signal is applied to the first grid of the electron gun and adjusts the focusing characteristics so as to stabilize the beam current. Because the cathode of the electron gun is operated at a negative potential, with respect to the faraday cage, it is necessary to isolate the control signal. Therefore the signal from the operational amplifier is used to modulate a 50 KHz carrier. The modulated signal is amplified and then demodulated in a capacity coupled diode demodulator, which is referenced to the cathode potential. After adequate filtering, to remove any remaining carrier signal, the control signal is applied to the first grid of the electron gun. A detailed diagram of the constant current control unit is displayed in Fig. 3. The ability of the device to regulate the beam current is dependent upon the fixed bias of the first grid and the focusing voltage placed upon the second grid. The short term current stability is better than .1% while the long term stability (e.g. 2 hours) is approximately 2%. For electron beam currents within the range of 5 to 40 microamperes the incident electrons have an energy distribution of 0.4 to 0.8 eV. The distribution is determined by retarding potential measurements and the appearance of fine structure in the excitation function of the 546.1 nm

transition of mercury. The appearance of such structure has been related to the energy distribution of the electron beam by S. Frisch⁽¹⁶⁾ and I. P. Zapesoch-ny⁽¹⁷⁾.

The collisional radiation passes out of the collision chamber at a right angle to the beam and is modulated at a frequency of 1 KHz by a mechanical chopper. The light is focused upon the slits of a 0.5 meter Ebert scanning monochromator, which selects a particular spectral transition for observation. The emerging light is detected by a high gain photomultiplier, placed in an evacuated cryostat which is attached to the monochromator.

The signal produced by the radiation from the excitation tube is of very low intensity, therefore one must employ a method of detection which enhances the signal to noise ratio of the information signal. The method employed in this investigation utilizes A.C. modulation techniques. The radiation from the collision chamber is modulated at 1KHz by a rotating wheel, with equally spaced holes. The output signal from the photomultiplier consists of high frequency pulses occurring in groups, whose frequency is determined by the mechanical chopper. The intensity of the light incident upon the photomultiplier determines the number of individual pulses which occur during an "on" period of the chopping cycle. However the amplitude of the individual pulses appears to be independent of the light intensity. Therefore an integrating amplifier is used to convert the photomultiplier signal to one whose amplitude is proportional to the intensity of the incident light. This is accom-

plished by integrating over each "on" period of the chopping cycle. The integrating preamplifier, shown in Fig. 4, consists of a low noise cascode preamplifier and an RC integrator, which creates a shaped wave whose amplitude varies with the photomultiplier signal. The values of R and C are selected so as to insure a linear response of the system for light signals of low intensity (i.e. low photomultiplier current). The stronger signals, which represent a greater number of events, will then be shaped in a similar manner. The signal is then amplified by an amplifier which is tuned to the modulation frequency of 1KHz, and has a gain of 60db. A detailed diagram of this device is displayed in Fig. 5. After sufficient amplification, which is controlled by means of an input attenuator, the signal is directed to a phase sensitive detector.

At the same time a 1KHz reference signal is created by a photocell, which detects the light from a small lamp placed diametrically opposite to the aperture, through which the radiation from the excitation tube passes. The reference signal is amplified and then fed to the phase sensitive detector, (c.f. Fig. 6). The signal from the tuned amplifier is selectively rectified by comparing it with the reference signal in a bridge network. The output from the bridge is proportional to the amplitude of the photo-multiplier signal. Maximum sensitivity is obtained by adjusting the phase of the reference signal so that it coincides with that of the photomultiplier signal, when they are applied to the bridge network. The remaining noise occurring in the D.C.

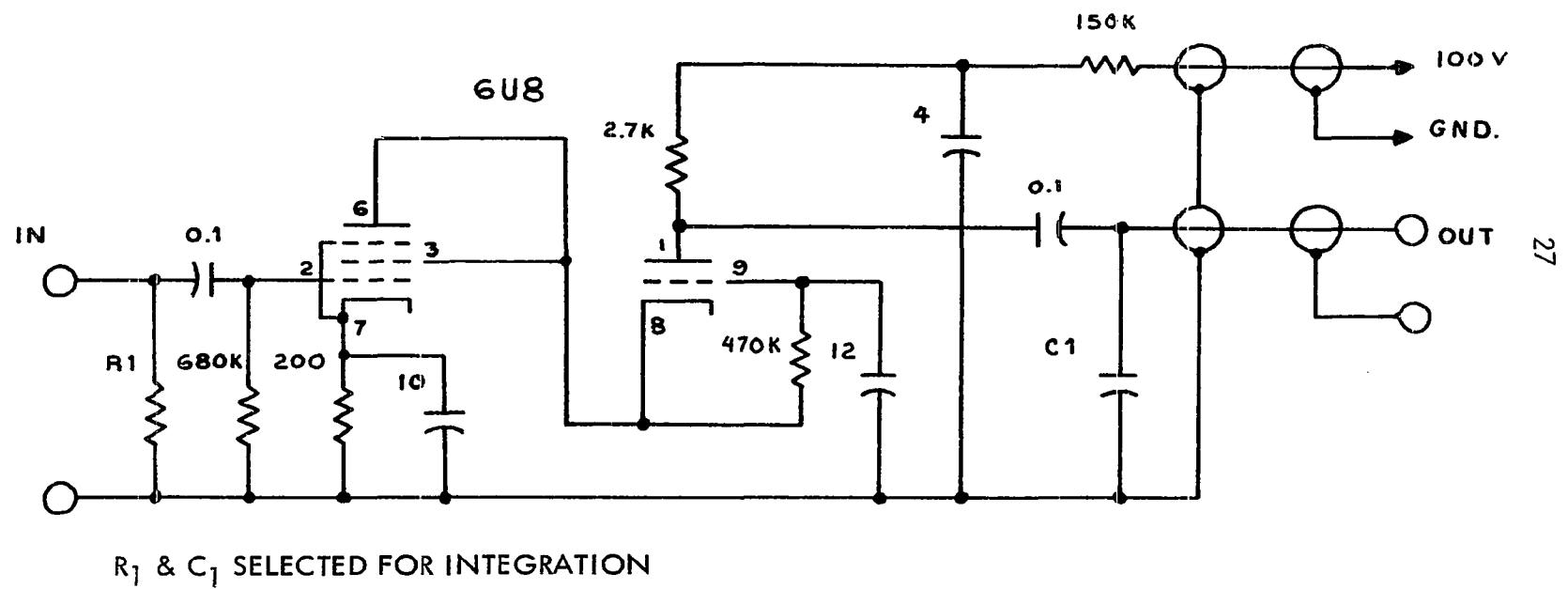


FIGURE 4. INTEGRATING AMPLIFIER.

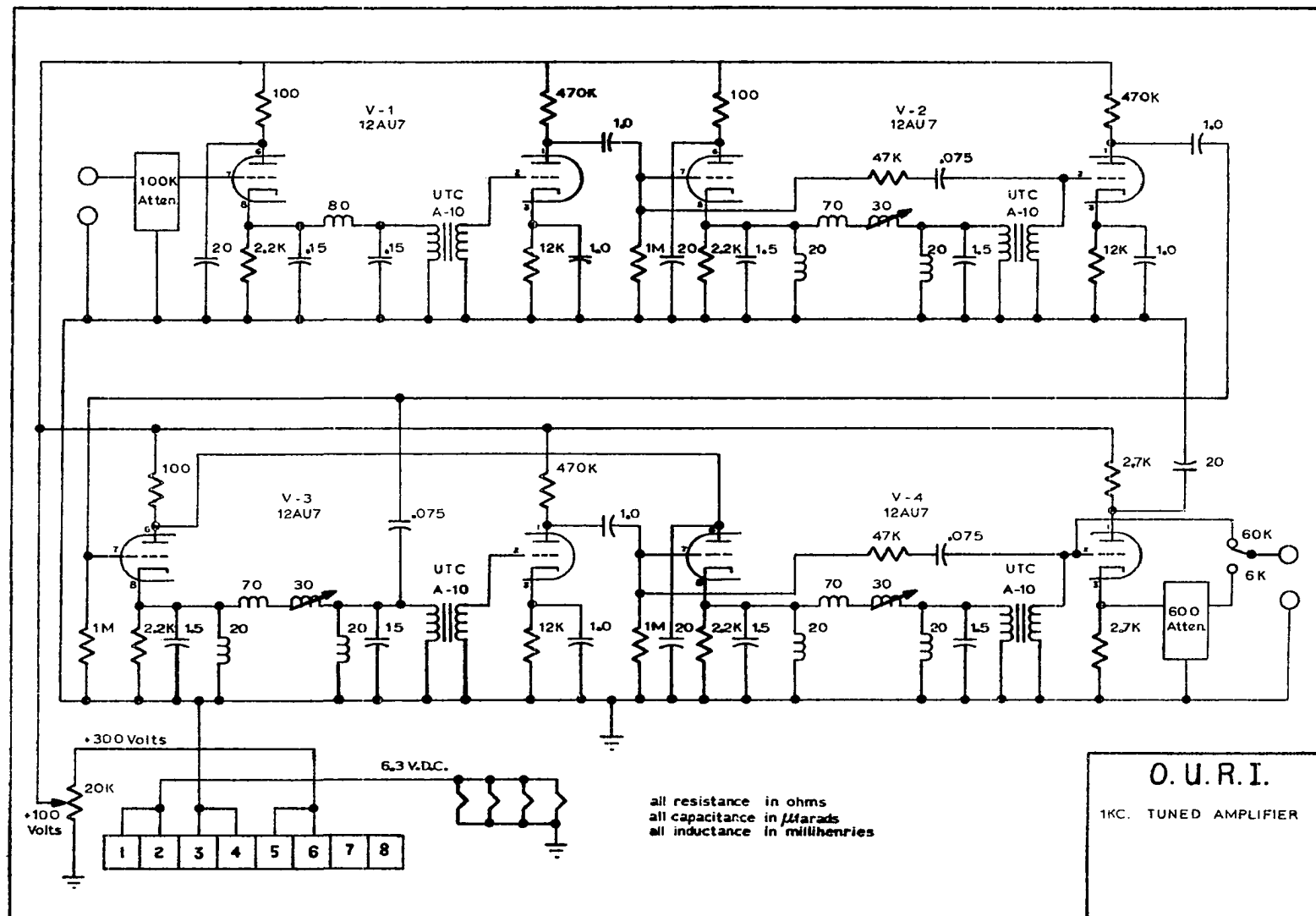


FIGURE 5. TUNED AMPLIFIER.

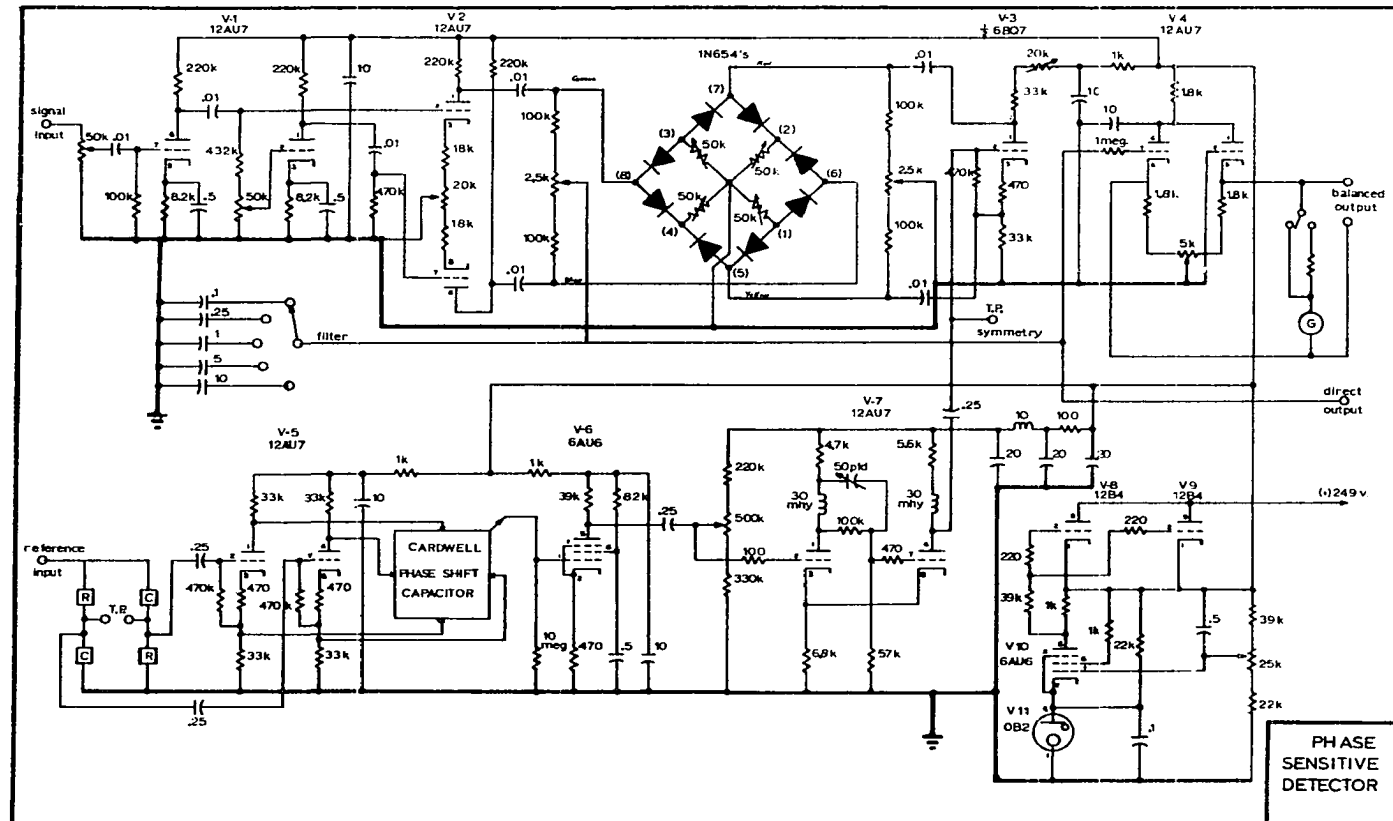


FIGURE 6. PHASE SENSITIVE DETECTOR.

output is reduced by passing the signal through a low pass filter. The output is then displayed on an x-y recorder as a function of incident electron energy, and is a relative measurement of the effective excitation cross at various electron energies.

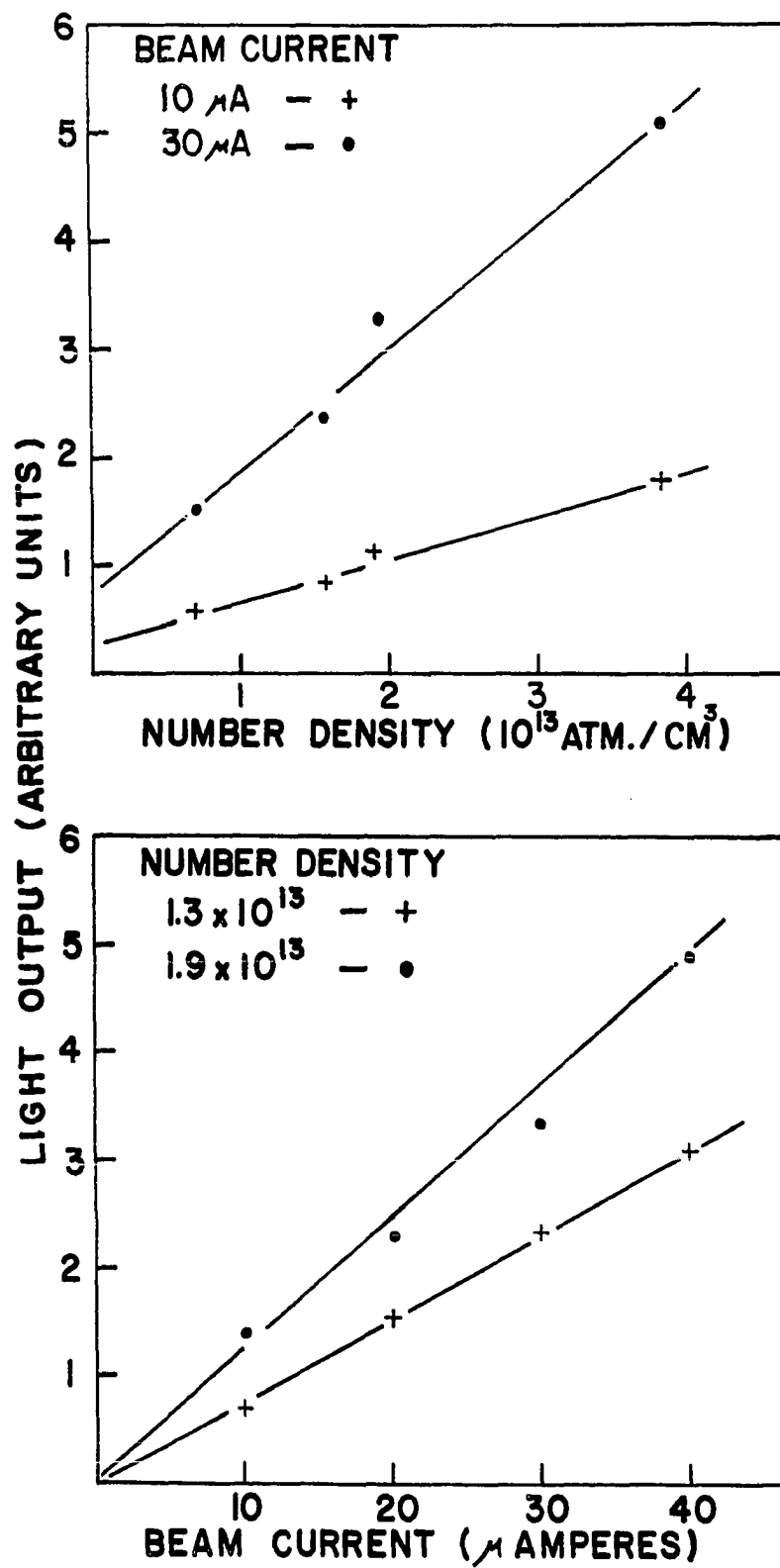
The entire electronic detection system was thoroughly checked and found to be a linear, with respect to the total range of photomultiplier signal, to within 3%. In addition it was determined that the signal output was linear with respect to variation of the entrance slit width of the monochromator over the slit range of .125 mm to 1 mm. Prior to making any measurements of the mercury spectrum, the radiative output of the excitation tube was recorded as a function of wavelength. This precaution allowed the identification of any spectral lines caused by impurity atoms. This procedure failed to uncover any impurity lines within the wavelength region of spectral interest

Optical Excitation Functions

Optical excitation functions for 40 transitions of the mercury spectrum were obtained in the manner described in the previous section. The curves were obtained under conditions of low electron beam current and low atom number density, e.g., $I \leq 30$ microamperes, and $N(g) \leq 4 \times 10^{-13}$ atoms/cm³. These precautions tended to insure the occurrence of single electron-atom collisions. The relationship between light output as a function of beam current and number density was observed for the $8^1P - 7^3S$ and $7^3S - 6^3P_{2,1,0}$

transitions and the results are displayed in Figs. 7 and 8. These transitions were chosen in part because the 8^1P level and the metastable $6^3P_{2,0}$ levels would be very sensitive to the reabsorption of radiation as it passes out of the chamber. In addition Fabrikant and Cirg⁽¹⁸⁾ have experimentally observed that stepwise excitation from the 6^3P_0 level has a large cross section for high electron densities, i.e. it is of the order of 10^{-16} cm^2 . Therefore the $7^3S - 6^3P_{2,1,0}$ transitions would be especially susceptible to a quadratic dependence upon current or pressure. The relationship between light output and beam current, (pressure), proved to be a linear in both cases for the range of beam current, (pressure), used in the experiment. On the basis of these results it was assumed that the remaining transitions would not exhibit a quadratic dependence since each was observed under the conditions which proved to be satisfactory for the critical 8^1P and $6^3P_{2,1,0}$ levels.

A discrepancy, corresponding to a few eV, exists between the theoretical and experimental onset potentials. This matter was thoroughly investigated by Jongerius, and was attributed to the influence of space charge, contact potentials, and field penetration. It was observed that these effects caused excitation functions to commence at a voltage which was larger than the theoretical onset by $2 \frac{1}{4} \pm \frac{1}{8}$ volts. The excitation functions presented in this work have been adjusted for the effects of contact potentials and field penetration by adjusting the experimental onset potential to coincide with the theoretical value. This corresponds to a constant shift of the voltage scale

FIGURE 7. CONTROL EXPERIMENTS; $8^1\text{P} - 7^1\text{S}$ (50 eV)

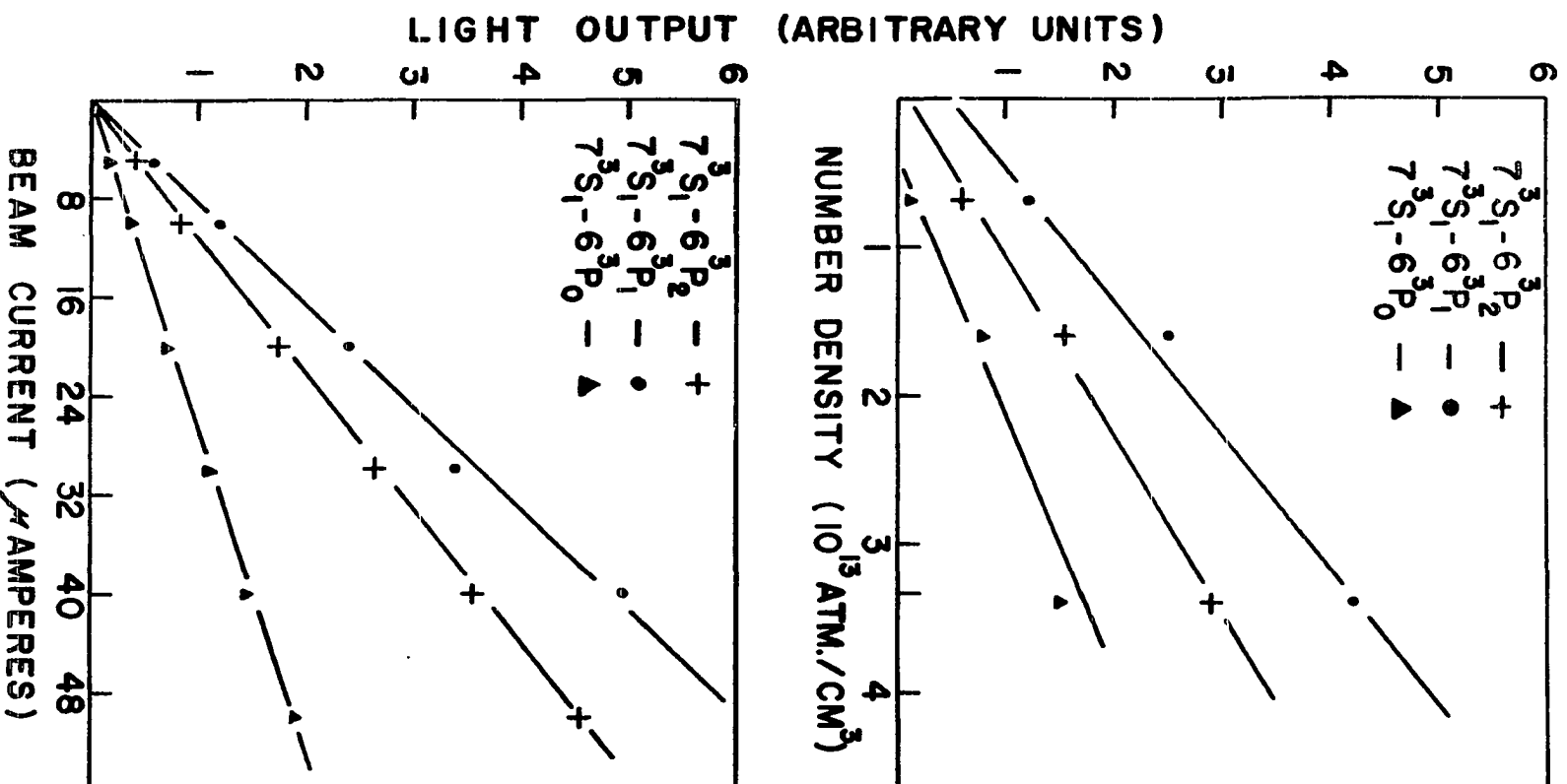


FIGURE 8. CONTROL EXPERIMENTS; $7^3S_1-6^3P_{2,1,0}$ (50 eV)

towards lower voltages. Because of the continuous nature of their acquisition, the curves have not been specifically corrected for space charge effects. However, this correction would only affect the voltage values at which the various maxima of the curves would occur, but not their relative heights.

When the observed transitions were adequately resolved from intense adjacent spectral lines, the various transition series usually exhibited similarly shaped curves. The complete resolution of the observed transitions was only possible for approximately 30% of the excitation functions. Many of the functions although not completely resolved, are of significantly greater intensity than the adjacent lines, and therefore present a nearly true representation of the desired excitation function. For many of the weaker transitions it was necessary to increase the resolution of the monochromator to ± 1.6 nm, hence their excitation functions are thoroughly distorted by the failure to isolate them from the lines of the ionized mercury spectrum and/or strong lines corresponding to normal or unassigned mercury transitions.

The lowest possible excited state for an ionized mercury atom has an onset potential of approximately 16 eV. Therefore one would expect no distortion of the excitation functions, due to the observation of Hg II lines, below this energy. The excitation functions of seven Hg II transitions have been observed by Schaffernicht ⁽¹⁹⁾ to possess a broad maximum occurring at either 55 or 90 eV., hence maximum distortion of the curves would occur at higher energies. Since the ionization cross section of mercury is relatively

large (of the order of 10^{-16} cm^2), there also exists the possibility that recombination processes make up a significant contribution to the population of the excited levels. Although no quantitative work has been carried out along this line, one observes distortions of some excitation functions at energies greater than the ionization potential (10.43 eV), but below the theoretical onset of the Hg II lines. It would be expected that the importance of an ionization recombination process, as a mode of population, would increase for states with large principal quantum number. The general characteristics of the excitation functions are described in the following sections. The non-principal lines will be discussed first so that one may attempt to form conclusions concerning their general shape. This necessity arises because many of the levels contribute, by cascade transitions, to the population of the states, which are of primary interest. The information gained through this examination will be used in the interpretation of the excitation functions of the 6^3D_3 , 6^3D_2 , 7^3S and 7^1S levels.

Triplet S and P Levels

The excitation functions corresponding to triplet levels n^3P ($n = 8, 14$) are displayed in Figs. 9 and 10. Many of the spectral lines of the $n^3P - 7^3S$ transition series were not resolved from adjacent lines of the Hg II and Hg I spectrum. Because of this, the shapes of the low intensity lines are distorted, thereby making it difficult to form very definite

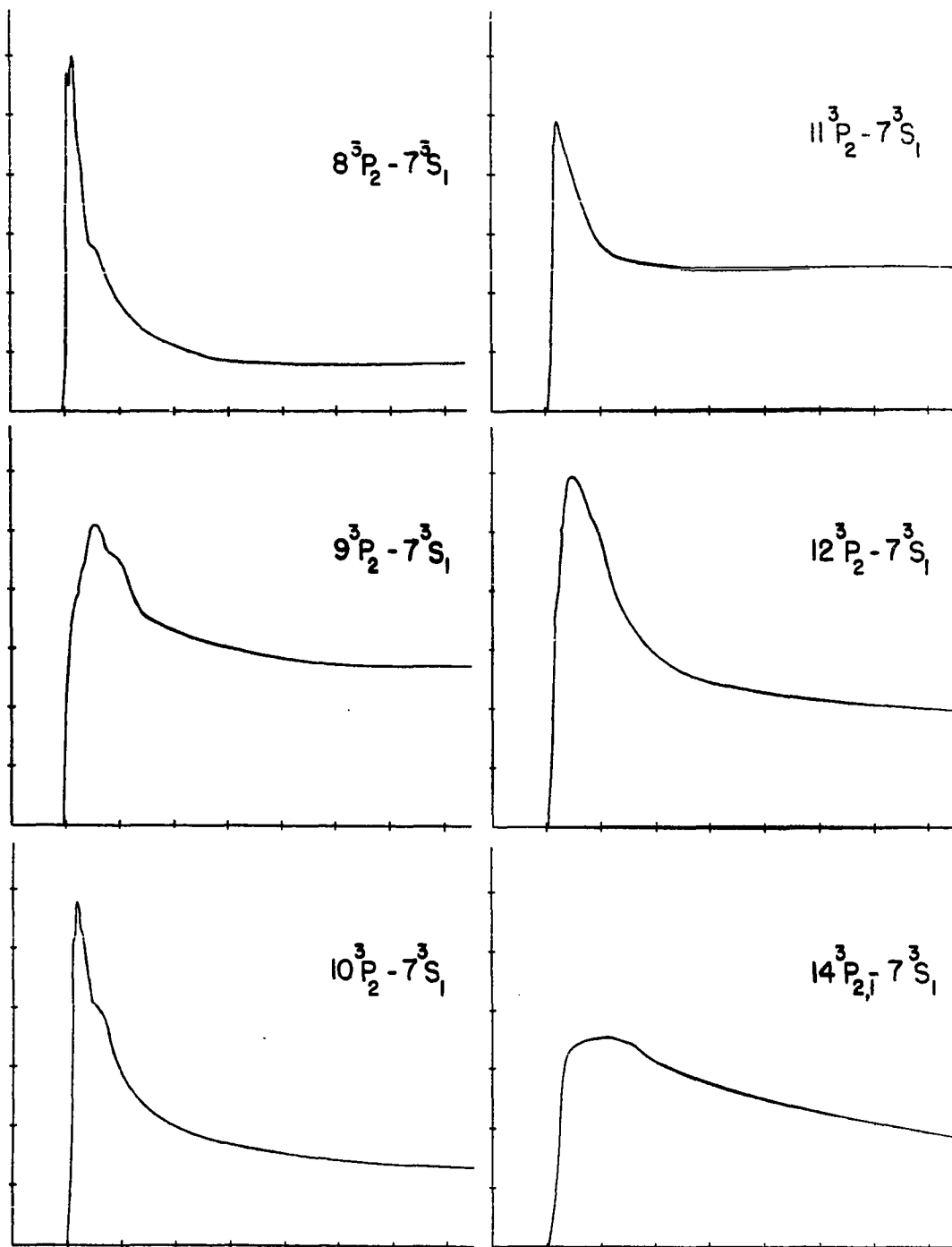


FIGURE 9. OPTICAL EXCITATION FUNCTIONS; $n^3P - 7^3S$ (0 - 90 eV)

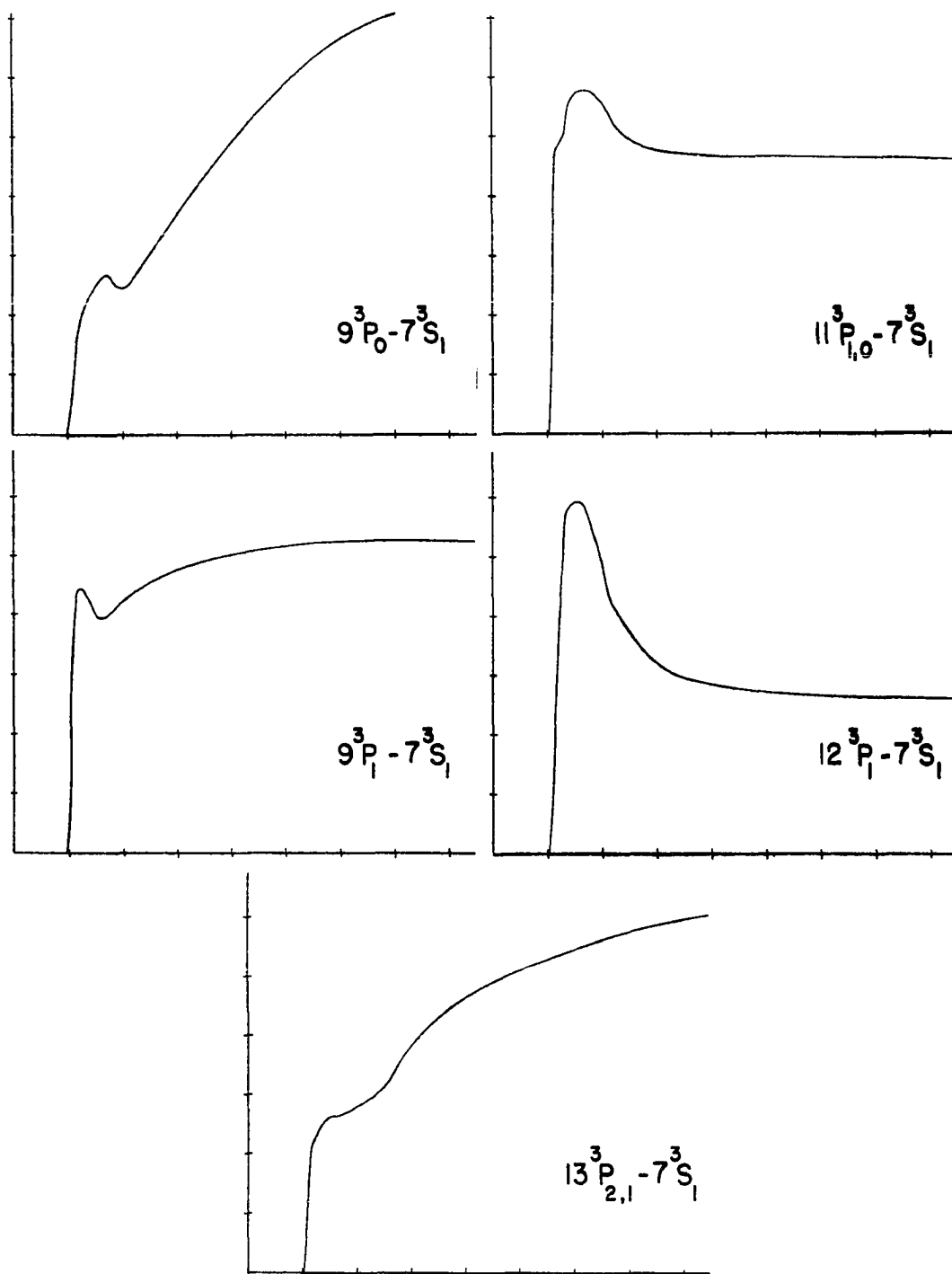


FIGURE 10. OPTICAL EXCITATION FUNCTIONS; $n^3P - 7^3S$ (0 - 90 eV)

conclusions concerning the general characteristics of the triplet excitation functions. However, the lines which are less susceptible to distortion, because of their proximity or intensity, exhibit the normal triplet characteristics. They possess steep maxima near the onset voltage and experience a rapid decrease with increasing electron energy. This shape is in agreement with that observed for the excitation functions of the triplet levels of helium.

Contaminating radiation, due to lack of resolution, was present for almost all of the observed transitions. Because of their relative intensities, the $8^3P_2 - 7^3S$ (690.7 nm) and $10^3P_2 - 7^3S$ (535.4 nm) transitions were least affected by the poor resolution, (e.g. the $8^3P_2 - 7^3S$ transition at 690.7 nm produced light which was approximately 25 times more intense than the adjacent lines at 692.4 nm and 689.7 nm). The excitation functions corresponding to the $9^3P_2 - 7^3S$ (582.1 nm), $11^3P_2 - 7^3S$ (512.1 nm), $12^3P_2 - 7^3S$ (498.1 nm) and $14^3P_{2,1} - 7^3S$ (482.7 - 483.2 nm) transitions experienced somewhat greater distortion. The 9^3P_2 function was not resolved from the Hg I line at 583.8 nm, while that of the 11^3P_2 level was observed together with an intense Hg II line occurring at 512.9 nm. In addition the 12^3P_2 and $14^3P_{2,1}$ levels yielded functions which were contaminated by the 498.1 nm and 482.6 nm lines of the Hg I spectrum. The excitation function of the 12^3P_1 (499.2 nm) level was resolved from all known Hg I and Hg II lines. It experienced a relatively sharp peak near its threshold, and decreased rapidly with increasing electron energy. The peak was much broader than that observed for the 8^3P_2 and

10^3P_2 curves. The broadening of the peak for levels of high principal quantum number may result from the extremely close spacing of the energy levels, and the finite energy distribution of the incident electrons. The curves representing the 9^3P_0 (587.2 nm), 9^3P_1 (585.9 nm), $11^3P_{1,0}$ (513.8 - 514.0 nm) and $13^3P_{2,1}$ (489.0 - 489.7 nm) transitions were thoroughly distorted because of the presence of numerous lines of the Hg II and Hg I spectrum, which were of comparable intensity and could not be resolved from the desired transitions. The transitions from these levels produced light which was of extremely low intensity, hence the curves experienced large distortions. However one does observe a peak occurring near the onset of each curve.

The n^3S levels also possess distinct maxima near the onset of their excitation functions. The excitation functions of the 8^3S , 9^3S , and 10^3S levels are displayed in Fig. 11. The $8^3S - 6^1P$ (502.5 nm) transition was totally resolved from adjacent lines, therefore one expects the curve to be a true representation of the excitation function. The trace exhibits a relatively sharp peak near its onset, but it does not experience a rapid decrease with increasing electron energy. At this time no valid explanation can be proposed for this apparent flat appearance. The $9^3S - 6^1P$ (414.0 nm) and $10^3S - 6^1P$ (381.6 nm) transitions were of low intensity, hence the true shape of the trace was readily distorted by the influence of neighboring Hg II and Hg lines. The excitation function of the 9^3S level was distorted by the presence of spectral lines occurring at 414.03 nm, 415.6 nm, 412.5 nm,

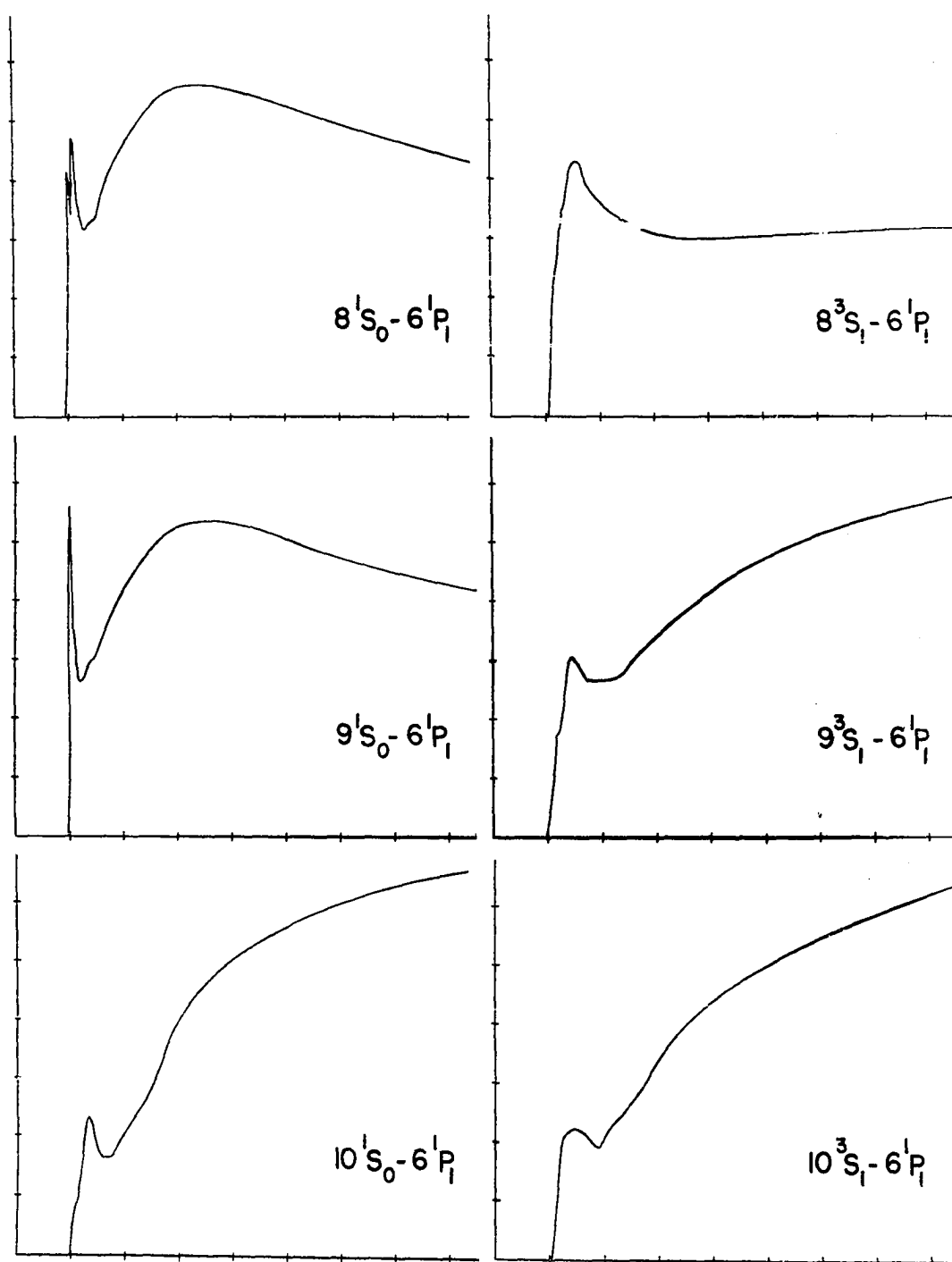


FIGURE 11. OPTICAL EXCITATION FUNCTIONS; $nS - 6P$ (0 - 90 eV)

and 412.0 nm, where the latter two belong to the Hg II spectrum. Similarly the curve of the 10^3S level was distorted by the failure to resolve it from an Hg line occurring at 382.0 nm, and a very strong Hg II line at 380.6 nm. However, in both cases the curves displayed maxima near their onset potential, which were characteristic of triplet levels.

Although many of the curves experience distortions, due to poor spectral resolution, one can propose that the triplet excitation functions generally possess a sharp maximum near their onset potential and decrease rapidly with increasing electron energy. The characteristic shape of the curves is similar to that which was observed for the triplet excitation functions of helium.

Singlet S and P Levels

The excitation functions of the n^1S and n^1P levels are displayed in Figs. 11-13. The excitation functions of the $n^1P - 7^3S$ and $n^1P - 7^1S$ transition series should exhibit similar shapes since the transitions emanate from a common upper level. Many of these curves were distorted by the presence of adjacent Hg and Hg II lines, which could not be resolved. Nevertheless the curves representing the 8^1P and 9^1P levels showed reasonable agreement. The $8^1P - 7^1S$ (671.6 nm) and $8^1P - 7^3S$ (607.3 nm) transitions yield curves which are slightly distorted by the presence of the 671.5 nm and 608.9 nm lines of the Hg II spectrum. Both curves exhibit a shallow peak near their onset which is followed by a broad peak occurring at approximately 20 eV. Likewise the $9^1P - 7^1S$ (623.4 nm) and $9^1P - 7^3S$ (567.6 nm)

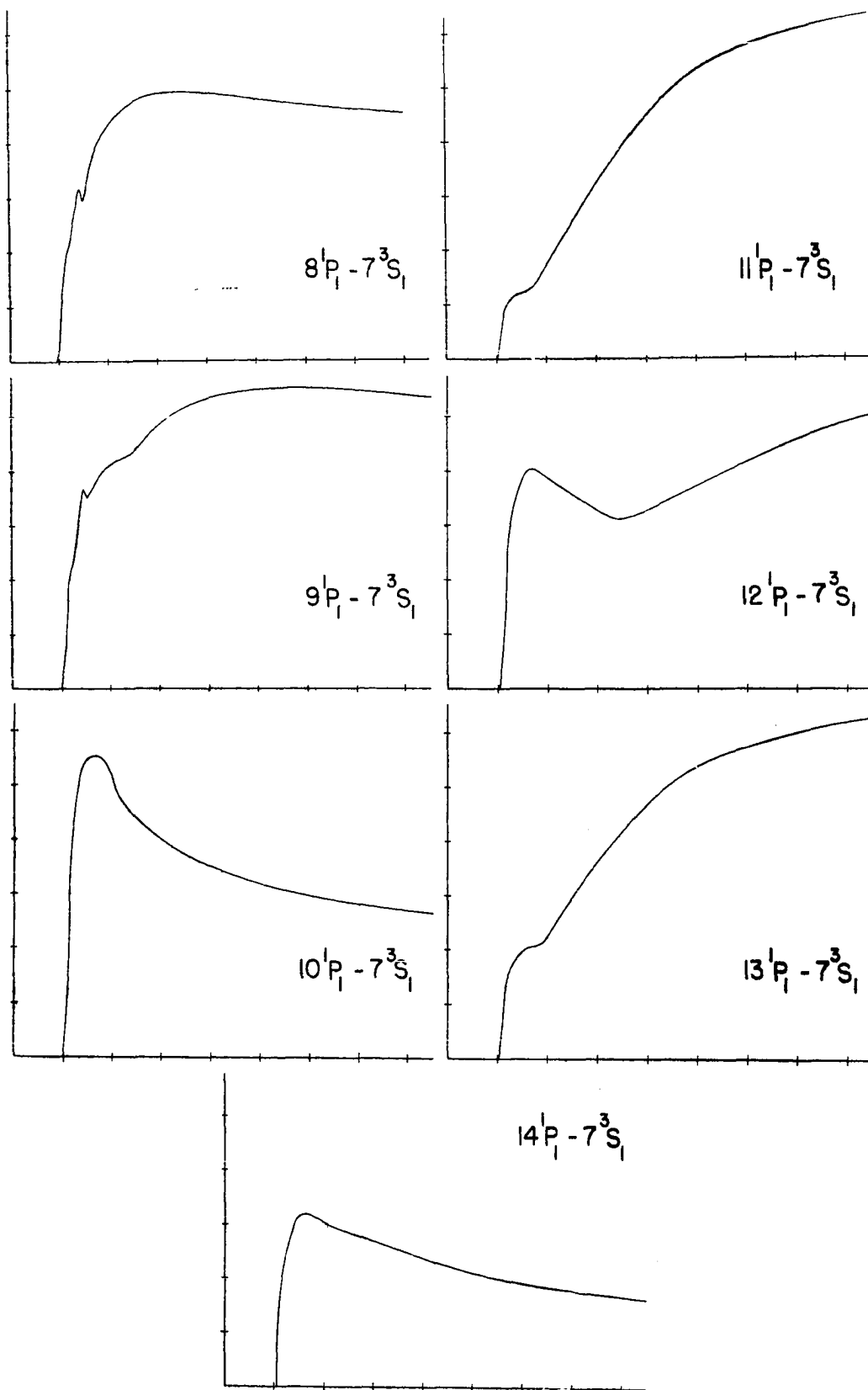


FIGURE 12. OPTICAL EXCITATION FUNCTIONS; $n^1P - 7^3S$ (0 - 90 eV)

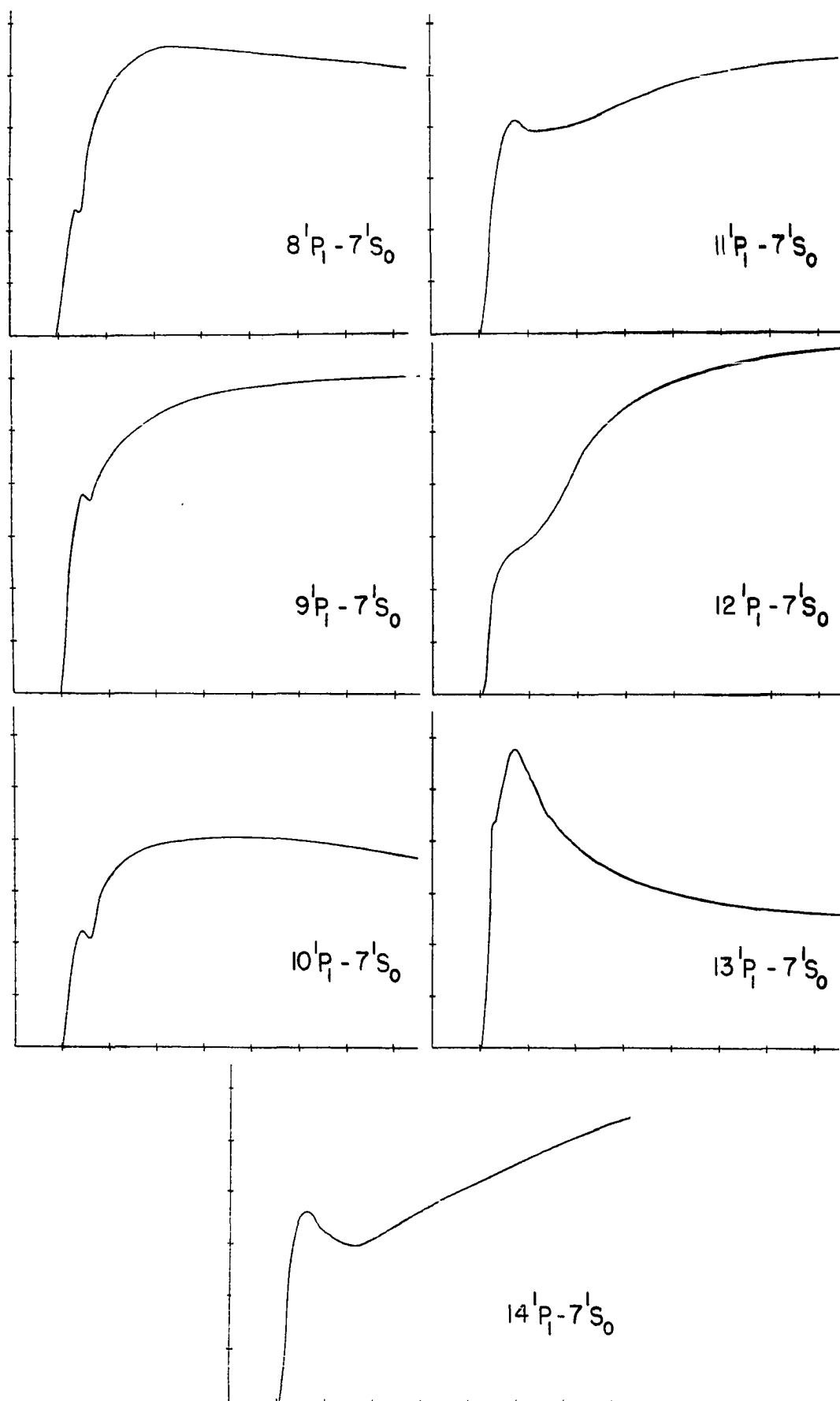


FIGURE 13. OPTICAL EXCITATION FUNCTIONS; $n^1P - 7^1S$ (0 - 90 eV)

transitions yielded curves which were of similar shape. The former transition was not resolved from the 624.2 nm and 622.0 nm lines of the Hg I spectrum, while the latter was distorted by a relatively intense Hg II line occurring at 567.7 nm. This similarity was not evident in the case of the $10^1P - 7^1S$ (580.3 nm) and $10^1P - 7^3S$ (531.7 nm) transitions. Both lines were observed under a condition of total resolution, hence they should be a true representation of the excitation function. One observes that the initial peaks occur at approximately the same energy and perhaps are the result of a common excitation mechanism. The broad peak experienced in the $10^1P - 7^1S$ transition does not materialize in the corresponding intercombination transition. This discrepancy can not be quantitatively explained, but one can suppose that its foundation lies in the singlet-triplet nature of the 10^1P level. The $11^1P - 7^1S$ (555.0 nm) and $11^1P - 7^3S$ (510.2 nm) transitions also exhibited a discrepancy in their relative structure. The former transition was not resolved from an Hg II line which occurs at 557.1 nm while the intercombination transition was resolved from all surrounding lines. Both curves exhibited a broad peak at approximately 80 eV. The reason for the great dissimilarity in their shapes is at this time still unknown. The excitation functions corresponding to the 12^1P and 14^1P levels were badly distorted for both transition series. The lines were of very low intensity and they could not be resolved from numerous Hg II lines which lay in the immediate vicinity. Also it was not possible to resolve the 12^1P function from those of the $10^3P_{1,0} - 7^3S$ transitions.

The transitions $13^1\text{P} - 7^1\text{S}$ (529.0 nm) and $13^1\text{P} - 7^3\text{S}$ (488.3 nm) yielded excitation functions which were distorted by the presence of the 529.4 nm Hg II line and the 489.0 nm Hg line respectively. The poor resolution caused the curves to exhibit a wide variation with respect to their relative shapes. The curve of the singlet transition possessed a relatively sharp peak at approximately 20 eV while the intercombination transition yielded a curve with a broad maximum at about 85 eV. This discrepancy can not be explained on the basis of previous experimental work.

The numerous discrepancies concerning the relative shapes of the $n^1\text{P}$ excitation functions, makes it difficult to form a general conclusion regarding the structure of a singlet curve. The states of large principal quantum number were especially susceptible to contradictions, however one notes good agreement for the curves representing the 8^1P and 9^1P levels. The structure of these curves is comparable to that observed by other investigators ⁽²⁰⁾. On the basis of this agreement it is proposed that the singlet levels are characterized by curves which possess broad maxima at energies of 2 to 5 times the onset voltage.

The excitation functions describing the $n^1\text{S}$ levels (Fig. 11) appear to possess both singlet and triplet characteristics. In addition to sharp peaks near their onset they also exhibit broad maxima appearing at higher excitation voltages. The excitation function corresponding to the $8^1\text{S} - 6^1\text{P}$ transition was isolated from the influence of all other spectral lines. It

possesses two sharp peaks, which occur at a sufficient energy above the threshold so as to create the speculation that they are the result of cascade transitions from the 8^3P_1 and n^3P_1 ($n \geq 9$) levels, which experience singlet-triplet mixing. The broad peak occurring at approximately 30 eV. is attributed to the direct excitation of the 8^1S level and cascade transitions from the n^1P levels. This analysis can be extended to the curve representing the $9^1S - 6^1P$ (410.8 nm) transition. This transition was not completely resolved from adjacent lines occurring at wavelengths of 411.5 nm (Hg II) and 410.3 nm (Hg). The initial sharp peak occurs at an energy above the threshold voltage, which is comparable to that required to excite the n^3P_1 levels. Therefore one may propose that it is the result of intercombination cascade transitions from the n^3P_1 levels. As in the previous case the trace exhibits a broad maximum occurring at approximately 30 eV and decreasing gradually thereafter. One notes a small shoulder appearing in both of the curves which occurs at approximately 15 eV. It is also noted that the excitation functions for the n^1P ($n = 8, 10$) levels exhibited diffuse peaks at approximately 12 to 15 eV, hence one may speculate that the structure of the n^1P curves is in part responsible for the appearance of the shoulder. The curve corresponding to the $10^1S - 6^1P$ (380.2 nm) transition experienced a large amount of distortion due to the presence of a strong line of the Hg II spectrum (380.6 nm). The curve exhibited a peak near its onset which was considerably broader than those discussed previously. The distortion due to the presence of the Hg II line prevents one from forming

very definite conclusions concerning its shape, at large electron energies.

D Levels

The excitation functions of the $n^1D - 6P$ series ($n = 6, 9$) could not be resolved from those of the $n^3D - 6P$ series. The curves representing the combined transitions are displayed in Fig. 14. The excitation function corresponding to the 8D level was distorted by the failure to resolve its spectral line from an intense Hg II line occurring at 391.4 nm. The remaining spectral lines were of sufficient intensity so as to insure that the shapes of the curves were true representations of the excitation functions, (e.g. the 6^3D_1 , $6^1D_2 - 6^3P_2$ transitions were 80 times more intense than the Hg I line occurring at 366.6 nm). All of the excitation functions exhibited maxima at approximately 15 eV to 20 eV and experienced a gradual decrease thereafter. The observed broad peak is characteristic of the singlet levels rather than of the triplet states. The energy distribution of the electron beam used in the experiment was too large to permit further resolution of the peaks. Although no firm conclusions can be drawn as to the roles of the various population mechanisms, one may speculate that the initial sharp peak of the 6^3D , 6^1D excitation function is produced by cascade transitions from the $3p$ levels.

Levels of Primary Interest

Four of the principal transitions of the mercury spectrum are considered in Fig. 15, which displays the excitation functions for the 7^3S , 7^1S ,

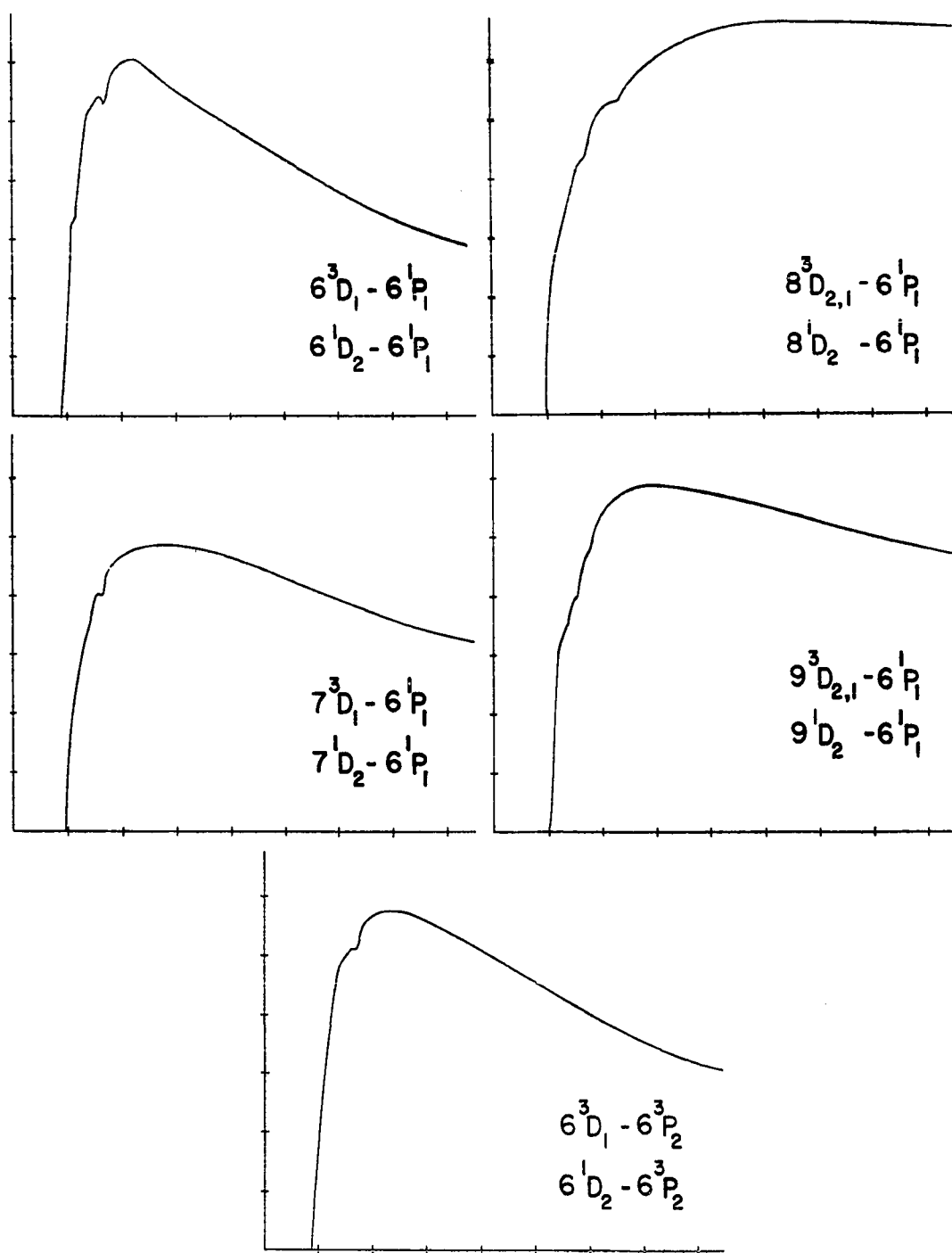


FIGURE 14. OPTICAL EXCITATION FUNCTIONS; $nD - 6P$ (0 - 90 eV)

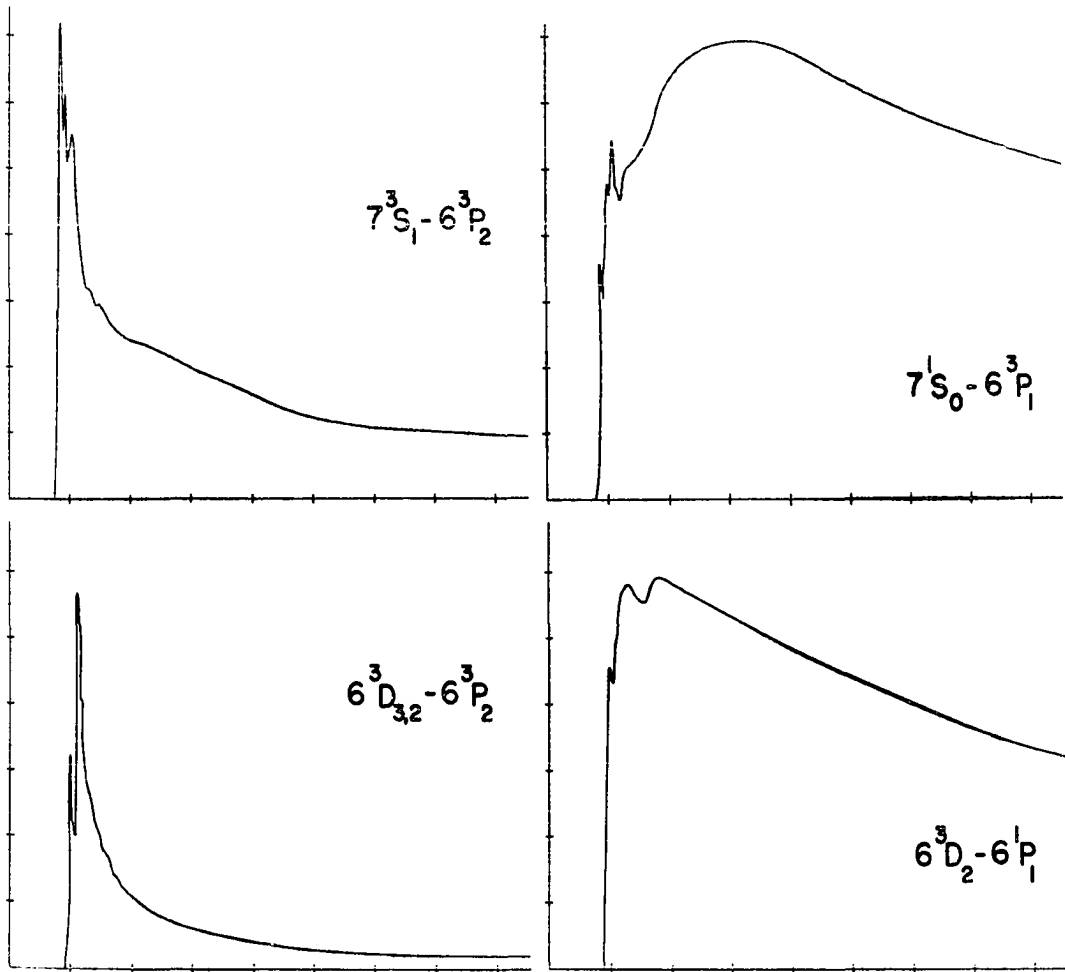


FIGURE 15. OPTICAL EXCITATION FUNCTIONS FOR THE TRANSITIONS
OF PRIMARY INTEREST (0 - 90 eV)

6^3D_2 , and 6^3D_3 levels. The excitation function should consist of a superposition of the electron excitation function for the initial level (e.g. 7^3S) and the excitation functions of all processes which tend to populate this level, (e.g. cascade contributions). The onset potential of each excitation function is unique, therefore the optical excitation function can be decomposed into curves, which represent the contributions to the population of the level under investigation.

The visible mercury triplet $7^3S - 6^3P_{2,1,0}$ has a common upper level, hence the excitation functions for the three transitions were observed to be similar. The 7^3S level produces an excitation function which possesses several sharp maxima near the onset potential and decreases rapidly thereafter. The shape of the curve was not influenced by adjacent spectral lines because of the extremely high intensity of the primary radiation, (e.g. the $7^3S - 6^3P_2$ radiation occurring at a wavelength of 546.1 nm is 400 times more intense than the adjacent 545.7 nm line). The fine structure of the curve is shown on an expanded energy scale in Fig. 16. The initial peak of the curve is attributed to the direct excitation of the 7^3S level by electron impact. This supposition follows from the fact that the incident electrons do not possess sufficient energy to excite the higher levels, which would ultimately populate the 7^3S state by cascade transitions. The energy difference between the first peak and the second pronounced peak corresponds to the energy difference between the 7^3S and 7^3P levels. This suggests that the structure is the result

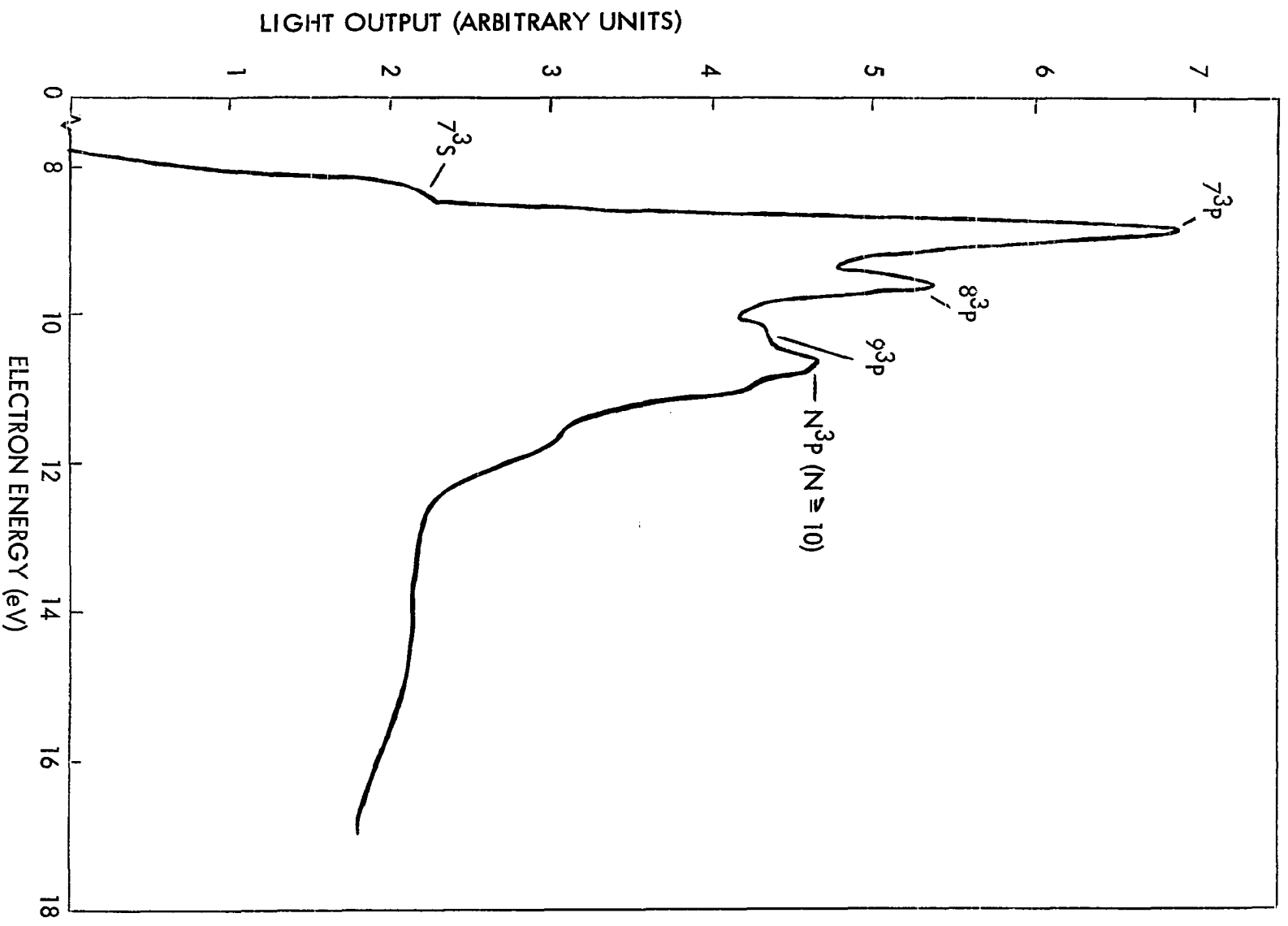


FIGURE 16. OPTICAL EXCITATION FUNCTION; $7^3S - 6^3P_2$ (0 - 18 eV)

of cascade transitions from the 7^3P levels. The peak is not further resolved because the $7^3P_{2,1,0}$ energy level spacing is less than the energy distribution of the incident electrons. The remaining peaks are analyzed in a similar fashion and attributed to cascade transitions from the nP levels ($n \geq 8$). There exists a diffuse peak at about 12 eV which is above the ionization potential of the atom, yet below the threshold of the lowest Hg II excited state, hence it may possibly be due to an ionization recombination process.

The structure of the optical excitation function of the $7^1S - 6^3P_1$ transition possesses sharp peaks near its onset potential, but also experiences a broad maximum which occurs at approximately 30 eV. The spectral line corresponding to this transition lies at a wavelength of 407.8 nm and could not be resolved from an adjacent Hg II line, which occurs at a wavelength of 408.1 nm. The Hg II line is considerably less intense than the primary line, hence the excitation function is a nearly true representation of the $7^1S - 6^3P_1$ transition.

The sharp peaks occurring near the curve's onset possess characteristics which have been attributed to triplet excitation functions. Since intercombination transitions from the n^3P_1 levels have a relatively large transition probability, one must examine this mechanism as a possible population mode for the 7^1S level. The first peak lies ~ 0.1 eV below the excitation threshold of the 7^3P_1 level, but one can not discount the possibility that it results from cascade transitions from this level. This possibility must be

considered because (1) the incident electrons possess a finite energy distribution (0.5 eV) which is comparable to the magnitude of the energy difference, and (2) the onset potential was adjusted so as to coincide with the theoretical value and hence it was not determined with sufficient accuracy to account for a discrepancy of a few tenths of an eV in the energy scale. The work of Jongerius has produced a $7^1S - 6^3P_1$ excitation function from which the energy difference, between the onset potential and the first peak, is determined to be 0.59 eV. This value is 0.13 eV less than the difference between that of the 7^1S and 7^3P_1 levels, and is comparable to the error limits placed upon the experimental value of the onset potential.

The second and third sharp peaks occur at energies above the onset, which are greater than the energies of the 8^3P_1 and 9^3P_1 levels with respect to that of the 7^1S level. Thus it is also possible that these peaks result from cascade transitions from the $3p_1$ levels.

The broad peak occurring at approximately 30 eV may result from the population of the 7^1S level by electron impact and cascade transitions from the n^1P levels. This supposition follows from the observations that the singlet P curves generally possessed a broad peak at higher energies, and that the maxima of the excitation functions for levels populated by a non-exchange mechanism are relatively broad.

A second intercombination transition is examined by considering the excitation function of the $6^3D_2 - 6^1P$ transition. The curve exhibits a

relatively sharp peak near the onset voltage and broader maxima at approximately 15 eV. The initial peak occurs at approximately 1.1 eV above the threshold voltage and possesses sharp triplet characteristics. Thus one may ascribe its presence to the population of the 6^3D_2 level by cascade transitions from the lower triplet P levels. The remaining broader maxima may be attributed to the fact that the 6^3D_2 level is mixed with the 6^1D_2 level, due to the presence of non-vanishing spin orbit coupling. The mixing allows the excitation function of the triplet D state to assume many of the characteristics peculiar to singlet levels (e.g. broader maxima).

The last primary transition to be considered is the $6^3D_3 - 6^3P_2$ transition which occurs at a wavelength of 365.0 nm. Because of the extremely close proximity of the $6^3D_2 - 6^3P_2$ transition (365.4 nm) there exists some doubt as to whether the curve was totally resolved, (it is estimated that a maximum of 25% of the 6^3D_2 light could have also been observed), therefore the two transitions are listed as corresponding to a single excitation function. With better resolution the $6^3D_2 - 6^3P_2$ transition was later observed to produce radiation which was approximately one tenth of the intensity of the $6^3D_3 - 6^3P_2$ transition at an energy of 15 eV. Therefore the excitation function corresponds primarily to the true excitation function of the 6^3D_3 level. The 6^3D_3 level does not experience singlet-triplet mixing, hence it is represented by a curve which exhibits narrow peaks near its onset potential and an extremely rapid decline thereafter. The level is populated

primarily through direct excitation by electron impact and cascade transitions from the n^3P_2 levels. The energy distribution of the electron beam was too gross to resolve the individual contributions.

Comparison with Other Investigators

The structure of the optical excitation functions, presented in the previous sections, is in general accord with that reported by other investigators. In numerous cases, the curves representing the n^3S , n^3P , and n^1P levels are distorted, due to inadequate spectral resolution. Nevertheless one observes that the triplet states are generally represented by excitation functions which possess steep maxima near their onset. This behavior has been observed by numerous investigators, to exist for collision processes which involve electron exchange, (i.e. the multiplicity of the excited state differs from that of the ground state atom). The excitation function of the 7^3S level exhibited several sharp maxima near its threshold. The appearance of the fine structure was in close agreement with that observed by Jongerius. Since the magnitude and resolution of the individual peaks are dependent upon the energy distribution of the incident electrons, the present results are in agreement only with those experimental results which were obtained under similar experimental conditions. A recent investigation of this structure by Zapesochny ⁽²¹⁾, utilizing an extremely univelocity electron beam (i.e. $\Delta V = 0.08$ eV), has extended the resolution of the various maxima displayed in this work. The lower singlet P states (i.e. small principal quantum number) are characterized by excitation

functions with shallow peaks near their onset and broad maxima at approximately 30 eV. The experiments of Thieme ⁽²²⁾ and Schaffernicht ⁽²³⁾ yield curves for the 8^1P and 9^1P levels which possess the broad maxima, but are devoid of the initial shallow peak. The excitation function for the $9^1P - 7^3S$ transition reported by Jongerius exhibits a slight plateau, occurring at an energy comparable to that of the shallow peak reported in this work. The failure of the early investigators to observe an initial peak may be attributed to a wide energy distribution of the incident electrons, which tended to mask the fine structure of the curves.

The relative shapes of the n^1S excitation functions presented in this work, exhibit excellent agreement with those reported by Schaffernicht ⁽²⁴⁾, Zapesochny ⁽²⁵⁾, and Frisch ⁽²⁶⁾. Schaffernicht presents an analysis of the population mechanisms which is in accord with that proposed in this investigation. By noting the energies at which the maxima occur, he is able to attribute the initial sharp peaks to the population of the n^1S levels by cascade transitions from the n^3P_1 levels. The invocation of intercombination cascade transitions allows him to account for the triplet character of the initial peaks. The broad peak occurring at approximately 30 eV is attributed to the direct excitation of the singlet levels. Conversely Frisch and Zapesochny propose that the initial sharp peak occurring in the excitation functions of the 7^1S , 8^1S , and 9^1S levels, is the result of direct excitation of the singlet levels. In addition they attribute the remaining peaks, occurring near the

curve's onset, to the effects of cascade transitions from the n^1P levels ($n \geq 7$). This supposition would require that the singlet excitation functions possess an extremely steep peak occurring near their onset voltage and a second diffuse peak at approximately 30 eV. For the case of the 7^1S level, they observed that the excitation function had an onset potential of 7.9 eV and exhibited its initial peak at 8.7 eV. Additional sharp peaks were observed at energies of 10.0 and approximately 11. eV. From the investigation of the 7^3S excitation function, it was noted that the 7^3P , 8^3P , and 9^3P levels yield excitation functions which are characterized by sharp peaks occurring at 8.9, 9.6, and 10.4 eV respectively. In addition, these levels possess respective threshold energies of 8.6, 9.4, and 9.8 eV. Therefore the peaks of the singlet curve occur at energies which are less than those of the triplet functions by 0.2 - 0.6 eV. On the basis of these facts it is concluded that the initial peak does not result from intercombination cascade transitions, (e.g. $7^3P_1 - 7^1S$). The 7^1P and 8^1P levels have critical potentials of 8.8 and 9.7 eV respectively and experience optically allowed transitions into the 7^1S level. Therefore it was proposed that the initial peak results from the direct excitation of the 7^1S level while the remaining peaks are caused by cascade transitions from the 7^1P and n^1P ($n \geq 8$) levels.

The error present in the determination of the energies at which the maxima occur was reported as ± 0.25 eV. This was attributed to the energy distribution of the incident electrons. In addition, the experimental onset

voltages of the curves were adjusted so as to coincide with the theoretical value by subtracting 2.3 ± 0.1 eV from the observed threshold voltage. One also notes that the curves were not adjusted for the effects of space charge. Its influence would tend to introduce a voltage correction, which is dependent upon the accelerating voltage of the electron beam (27). The analysis proposed by Frisch and Zapesochny is dependent upon energy differences of 0.2 - 0.5 eV, which are comparable to the error present in the voltage measurements. Therefore on the basis of the cited work, one can not definitely discard the possibility that the sharp maxima result from intercombination cascade transitions (e.g. $7^3P_1 - 7^1S$).

The relative shape of the excitation function corresponding to the $6^3D_3 - 6^3P_2$ transition, showed excellent agreement with the curve obtained by Jongerius. The 6^3D_3 level does not experience singlet-triplet mixing, therefore the curve exhibited the characteristic triplet shape, (i.e. sharp peak near the onset and a rapid decrease thereafter). The two distinct maxima were not resolved in the early experiments of Schaffernicht, but instead were fused into a single steep peak occurring immediately after the onset of the curve. The excitation functions for many of the $n^3D_{2,1}$ and n^1D_2 levels were not resolved in this work. The intercombination transition $6^3D_2 - 6^1P$ was investigated in order to obtain the excitation function of the 6^3D_2 level. The shape of the curve was in general agreement with that reported by Jongerius, Thieme and Schaffernicht. The latter author suggests

that the initial sharp peak is the result of direct excitation by electron impact, while the broad maximum is indicative of strong intercombination transitions from the n^1P levels. The curve presented in this work does not yield information which would contradict this analysis. Yet one must also note that the 6^3D_2 state is a mixture of singlet and triplet components, thus the broad maxima may represent the singlet structure of the level.

The excitation functions of the $n^3D_{2,1}$ levels could not be resolved from those representing the n^1D_2 levels. Therefore the resultant curves exhibited dominant singlet characteristics (e.g. broad peaks at 20 - 30 eV). These levels were resolved by Schaffernicht who reported that both the n^3D_2 and n^1D_2 states were characterized by curves which possessed broad maxima at approximately 30 eV. The failure of the n^3D_2 levels to exhibit the normal triplet characteristics lies in the mixed nature of the state. Thus the curves possess characteristics which are representative of the singlet component of the level. It was also observed, by Schaffernicht, that the unmixed n^3D_1 states were characterized by curves which possessed sharp maxima near their onset, and decreased rapidly thereafter.

CHAPTER IV

ABSOLUTE MEASUREMENTS

Absolute measurements of the effective excitation cross section, $Q(j,k)$, for a spectral line, can be determined through a direct comparison with a calibrated tungsten ribbon source. The cross section is proportional to the rate of spectral emission from the j th excited level, and is defined as

$$Q(j,k) = \frac{J(j,k)}{I/eN(g)} , \quad (25)$$

where $J(j,k)$ is the rate of photons emitted per cm of beam, I is the electron beam current, $N(g)$ is the number density of the ground state atoms, and e is the electronic charge. The electron beam current is readily measured and the number density of the ground state atoms follows from the ideal gas law. Therefore it is necessary to devise a method which will insure an accurate measurement of the rate of photons emitted, per unit beam length, in the $j \rightarrow k$ transition.

Experimental Procedure

The radiation emitted by the excited atoms undergoing transitions leaves the excitation tube at a 90° angle to the electron beam. It is focused with unit magnification, horizontally upon the slits of the monochromator. The imaging lens possesses a suitable field stop so that the image just fills the rectangular grating of the monochromator. This procedure insures that all of the light entering the entrance slit will be detected, therefore the influence of scattered light will be minimized. The emerging light totally illuminates the cathode surface of a high gain photomultiplier tube, which is placed directly in front of the exit slit. This geometry eliminated the introduction of inaccuracies due to sensitivity variations over the cathode surface. Thermal noise was reduced by cooling the photo tube to -178°C , and additional noise (e.g. fluorescence of the inner walls) was minimized by operating the cathode at ground potential. These precautions allowed the signal to noise ratio to be maintained at a value greater than five, for even the weakest signals. The photomultiplier output was measured by a D.C. microammeter, which was modified to operate at 2 Kv above ground potential. In addition, the measurements were taken at large incident electron energies (e.g. 50 eV) so that small variations in the incident electron energy would not introduce significant changes in the radiative output.

The spectral transitions were observed at wavelength resolutions of ± 0.2 , ± 0.4 , and ± 1.6 nm, corresponding to slit widths of $\frac{1}{8}$, $\frac{1}{4}$, and 1 mm respectively. The effective solid angle, through which the beam's

radiation is collected by the monochromator, is equal to the area of the system's entrance pupil divided by the square of the distance from the beam to the pupil. The area is determined by employing a series of diaphragms, of various diameters, as aperture stops. The ratio of the effective pupil area to the area of the aperture stop is equal to the ratio of the intensity of the unobstructed light to the intensity of that which passes through aperture stop. The latter ratio was directly proportional to the square of the aperture stop diameter. The actual number of photons which are detected by the photomultiplier, at a right angle to the electron beam, is proportional to the photomultiplier signal and to the spectral response of the detection system. This condition is expressed through the equation

$$J(j,k) = \frac{4 \pi C(\lambda) \cdot I(cc)}{\Omega(cc) T(\lambda)} \quad , \quad (26)$$

where $\Omega(cc)$ is the effective solid angle subtended by the collision chamber, $T(\lambda)$ is the transmissivity of the optical system, $C(\lambda)$ denotes the photon efficiency of the photomultiplier tube, and $I(cc)$ is the photomultiplier current. The efficiency of the photomultiplier tube is determined, as a function of wavelength, by direct comparison with a tungsten ribbon lamp, manufactured and calibrated by the General Electric Company. The number of photons, emanating from the ribbon lamp, which are incident upon the photocathode will be proportional to $C(\lambda)$, and to the photomultiplier signal, $I(sl)$. The D.C. current through the ribbon was adjusted so that the source acquired

true brightness temperatures of 1500, 1550, and 1600°K. The quantity $J(s)$ is defined as the rate of emission of photons from a unit area of the ribbon into a unit solid angle normal to its surface. This quantity was calculated by employing Planck's radiation law and the emissivity coefficients of tungsten, reported by Larabee (28). The light from the ribbon lamp was focused upon a small rectangular aperture, whose dimensions and optical distance corresponded to those of the electron beam. After leaving the aperture the light passes through a right angle prism and is focused upon the monochromator slit. Thus the light incident upon the slit comes from a small area of the tungsten ribbon which can be determined from the magnification properties of the optical system. The total rate of emission of photons normal to the ribbon is given by the product of three quantities, (1) the rate of photon emission per cm^2 per steradian, $J(s)$, (2) the effective area of the ribbon, $A(s)$, and (3) the solid angle subtended by the standard lamp lens, $\Omega(s)$. Since the rate at which photons are incident upon the photomultiplier is proportional to the resulting signal, one obtains the expression

$$J(s) = \frac{C(\lambda) I(s)}{\Omega(s) A(s) T'(\lambda)} \quad (27)$$

where $T'(\lambda)$ is the transmissivity of all optical devices which are employed in the standardization process, and $I(s)$ is the photomultiplier signal. In this manner $C(\lambda)$ is determined in terms of experimentally determinable quantities. Therefore the rate of photons, emitted per cm of electron beam, is

given as

$$J(j, k) = 4 \pi J(s) A(s) \cdot \frac{\Omega(s)}{\Omega(cc)} \cdot \frac{T(\lambda)}{T(\lambda)} \cdot \frac{I(cc)}{I(s)} \quad (28)$$

The ratio of the transmissivities of the two optical systems reduces to the transmissivity of the lens-prism combination, which is unique to the standardization system. This quantity was determined, as a function of wavelength, by calculating the value for wavelengths greater than 500 nm and employing relative measurements to determine the functional relationship.

The measurement of the cross section corresponding to the transitions $7^3P_2 - 7^3S$ (1128.7 nm) and $7^1S - 6^1P$ (1013.9 nm) were obtained by replacing the photomultiplier tube with a camera and using type I-Z Kodak spectroscopic plate as the detector. The type I-Z emulsion was hypersensitized so as to extend its sensitivity to 1200 nm. The plate was attached to the exit slit of the monochromator and adjacent portions of it were exposed by the two sources for equal periods of time. The standard lamp was operated at a true ribbon temperature of 1200°K so that its intensity would be comparable to that of the collisional radiation. The values of the emissivity of tungsten at 1200°K were obtained by extrapolating the emissivity data of J. C. DeVos (29). The plate was processed immediately after its exposure and the photographic density of the two images was determined. The difference in photographic density is related to the intensity ratio of the two sources and

hence provides the means of comparison.

Effective Excitation Cross Sections

In this manner, measurements were made of the effective excitation cross sections for 45 spectral transitions of mercury. The measurements were made at an incident electron energy of 50 eV and the optical excitation functions were used to determine the values at an energy of 15 eV. The results of the absolute measurements are grouped according to their transition series and are presented in Tables III-VIII. Limits of experimental error are placed upon the values on the basis of two criteria (1) experimental repeatability and (2) readability of the measuring devices. The error introduced into the determination of the number density is estimated at 3%. This estimate is an upper limit and takes into account the possibility that the collision region is up to 6°C warmer than the prevailing room temperature, (thermionic measurements by Hanle ⁽³⁰⁾, made under similar conditions, have shown temperature differences of approximately 3°C). The electron beam current was known to 1% accuracy and the photomultiplier output was judged to be accurate to within 2% for strong lines and to within 15% for extremely weak spectral lines. The error introduced by uncertainties in the ribbon lamp properties (e.g. emissivity of tungsten) and through the measurements of the optical constants (e.g. solid angles and transmissivity) are mutually independent and therefore should be combined quadratically. This analysis results in an estimate which lies below the repeatability of the measurements, therefore the limits of accuracy are determined

TABLE III
EFFECTIVE EXCITATION CROSS SECTIONS $n^1P - 7^1S$

Wavelength (nm)	Upper Level	$Q(j,k)$ at 15 eV (10^{-19} cm^2)
671.6	8^1P	9.2 ± 1.3
623.4	9^1P	6.5 ± 1.2
580.3	10^1P	0.83 ± 0.17
554.9	11^1P	0.43 ± 0.08
539.3	12^1P	0.27 ± 0.04
529.0	13^1P	0.25 ± 0.06
521.9	14^1P	0.15 ± 0.04

TABLE IV
EFFECTIVE EXCITATION CROSS SECTIONS $n^1P - 7^3S$

Wavelength (nm)	Upper Level	$Q(j,k)$ at 15 eV (10^{-19} cm^2)
607.2	8^1P	5.4 ± 0.8
567.6	9^1P	4.3 ± 0.7
531.7	10^1P	1.3 ± 0.2
510.2	11^1P	0.13 ± 0.03
497.0	12^1P	0.14 ± 0.03
488.3	13^1P	0.19 ± 0.04
482.2	14^1P	0.16 ± 0.04

TABLE V
EFFECTIVE EXCITATION CROSS SECTIONS $n^3P - 7^3S$

Wavelength (nm)	Upper Level	$Q(j,k)$ at 15 eV (10^{-19} cm^2)
546.1	6^3P_2	70 ± 8
435.8	6^3P_1	59 ± 6
404.7	6^3P_0	19 ± 2
1128.7	7^3P_2	250 ± 80
690.7	8^3P_2	4.1 ± 0.6
582.1	9^3P_2	0.34 ± 0.08
585.9	9^3P_1	0.44 ± 0.08
587.2	9^3P_0	0.31 ± 0.07
535.4	10^3P_2	0.40 ± 0.08
538.5-538.9	$10^3P_{1,0}$	0.09 ± 0.02
512.1	11^3P_2	0.39 ± 0.06
513.8-514.0	$11^3P_{1,0}$	0.21 ± 0.05
498.1	12^3P_2	0.30 ± 0.07

TABLE V Continued

499.2	12^3P_1	0.21 ± 0.05
489.0-489.7	$13^3P_{2,1}$	0.16 ± 0.04
482.7-483.2	$14^3P_{2,1}$	0.18 ± 0.04

Note: The cross section for the $10^3P_{1,0} - 7^3S$ transitions was resolved from that of the $12^1P - 7^1S$ transition.

TABLE VI

EFFECTIVE EXCITATION CROSS SECTIONS: $nS - 6^1P$

Wavelength (nm)	Upper Level	$Q(j,k)$ at 15 eV (10^{-19} cm^2)
1013.9	7^1S	$64. \pm 1.3$
491.6	8^1S	$11. \pm 1.5$
410.8	9^1S	2.7 ± 0.3
380.2	10^1S	0.72 ± 0.11
502.5	8^3S	0.15 ± 0.06
414.0	9^3S	0.10 ± 0.03
381.6	10^3S	0.15 ± 0.05

TABLE VII

EFFECTIVE EXCITATION CROSS SECTIONS $nD - 6^1P$

Wavelength (n m)	Upper Level	$Q(i,k)$ at 15 eV (10^{-19} cm^2)
579.0-579.1	$6^3D_1, 6^1D_2$	$42. \pm 5.$
577.0	6^3D_2	$28 \pm 3.$
434.3-434.7	$7^3D_2, 7^1D_2$	$18 \pm 3.$
390.1-390.3-390.6	$8^3D_{2,1}, 8^1D_2$	4.8 ± 0.8
370.1-370.2-370.4	$9^3D_{2,1}, 9^1D_2$	1.2 ± 0.2

TABLE VIII

EFFECTIVE EXCITATION CROSS SECTIONS $nD - 6^3P_2$; $n^1S - 6^3P_1$

Wavelength (nm)	Upper Level	$Q(j,k)$ at 15 eV (10^{-19} cm^2)
365.0	6^3D_3	75 ± 13
365.5	6^3D_2	5.9 ± 1.2
366.3	$6^3D_1, 6^1D_2$	$5.7 \pm 1.$
407.8	7^1S	$13. \pm 1.5$

by the experimental repeatability.

The repeatability of twelve ribbon lamp calibration measurements varied within the limits of 2 to 10%, with the larger variation occurring for regions of low detection sensitivity.

Comparison with Other Investigators

The effective cross sections, (e.g. Tables III to VIII) , presented in this work are compared to those determined by Jongerius, Hanle, and Thieme. The measurements are compared at the electron energies reported by the authors, in order to minimize the introduction of inaccuracies. The measurements of Jongerius are reported at an incident energy of 15.4 eV while those of Hanle and Thieme are reported at 60 eV. The shapes of the optical excitation functions were employed to normalize our values to these energies. Table IX displays the absolute measurements of the four experiments.

The absolute cross sections of the present work are consistently larger than those reported by Jongerius, with the exception of the $6^3D_3 - 6^3P_2$ and $6^3D_1, 6^1D_2 - 6^3P_2$ transitions. The percentage of differences ranges from 8 to 65 per cent, and lies outside of the reproducibility limits placed on the separate measurements. On the other hand the measurements of Hanle and Schaffernicht, and those of Thieme at 60 eV are from approximately 2 to 4 times larger than those of the present work. The appearance of a wide range of disagreement in the comparison suggests the absence of a systematic experimental error in the results of the present work.

TABLE IX

COMPARISON OF EFFECTIVE EXCITATION CROSS SECTIONS

All cross sections are expressed in units of 10^{-19} cm^2

Transition	Q(j,k) at 15 eV		Q(j,k) at 60 eV		
	This Work	Jongerius	This Work	Hanle and Schaffernicht	Thieme
$7^3S - 6^3P_2$	70 ± 7	45 ± 5	25 ± 3	67	57
$7^3S - 6^3P_1$	59 ± 6	36 ± 4	21 ± 2	82	--
$7^3S - 6^3P_0$	19 ± 2	13 ± 1.3	$6.8 \pm .7$	38	31
$7^1S - 6^3P_1$	13 ± 1.5	9.6 ± 1	14 ± 2	--	56
$8^1S - 6^1P$	11 ± 1.5	8.4 ± 0.9	16 ± 2.1	--	20
$9^1S - 6^1P$	2.7 ± 0.3	2.0 ± 0.25	4.1 ± 0.5	--	9.4
$8^1P - 7^3S$	5.4 ± 0.8	--	7.0 ± 1.0	--	18
$9^1P - 7^3S$	4.3 ± 0.7	3.0 ± 0.4	6.9 ± 1.0	13	--
$6^3D_3 - 6^3P_2$	75 ± 13	78 ± 9	9.5 ± 1.7	--	--
$6^3D_2 - 6^1P$	28 ± 3	24 ± 3	20 ± 3	52	58
$9^1P - 7^1S$	6.5 ± 1.2	--	10 ± 2	--	25

TABLE IX Continued

$6^1D_2 - 6^1P$ 6^3D_1	42 ± 5	36 ± 4	30 ± 4	105	92.
$6^3D_1 - 6^3P_2$ 6^1D_2	5.7 ± 1	6.3 ± 1.2	--	--	--

The measurements of Hanle and Schaffernicht were made with an electron beam current of $445 \mu\text{A}$ and with a saturated mercury vapor pressure corresponding to 26°C . The radiation was detected by a photo cell, and a Hefner candle was used as a standard light source. The data was presented in terms of the number of light quanta passing through a unit area, (1cm^2), at a perpendicular distance of 1 meter from the beam. The measurements were reported for 1 cm of beam length, 10^{-10} amperes of beam current, 10^{-3} Torr Hg pressure and an electron energy of 60 eV. The measurements of Thieme were normalized to the absolute value of the $7^3\text{S} - 6^3\text{P}_1$ cross section reported by Hanle and Schaffernicht. Therefore the two experiments were not mutually independent. Fischer (31) measured the absolute cross section of the $7^3\text{S} - 6^3\text{P}_1$ transition under more favorable experimental conditions (e.g. a beam current of $41 \mu\text{A}$ and a vapor pressure corresponding to 19°C). Employing a ribbon lamp as a standard source he measured a value which was approximately 2.6% smaller than that reported by Hanle. The values of the absolute cross sections are very sensitive to the calibration procedure (i.e. the determination of the detector sensitivity). Therefore one could speculate that the larger cross sections resulted from errors in the absolute calibration. This supposition is supported by the fact that Thieme's excitation cross section measurements for helium exhibit serious disagreement with the more recent measurements. Thieme's measurement of the 3p cross section at its peak value is approximately 20 times larger than that reported by Miller (32). The description

of the calibration procedure, in the cited works, did not provide a sufficient insight to the procedure so that the origin of the discrepancy could be located.

The absolute measurements reported by Jongerius are much smaller than those of the early experimentors. Jongerius employed technological advancements in his experimental technique which are similar to those used in this work, (e.g. high gain photomultiplier detector). The experiments employed similar methods for determining the absolute cross sections, with the exception of the calibration procedure. Jongerius replaced the excitation tube by the ribbon lamp which produced recorder indications which were 10^4 to 10^5 times larger than those produced by the collisional radiation. This ratio was reduced by employing smaller than usual fixed monochromator slits, and neutral density filters during the ribbon lamp exposure. Nevertheless a typical measurement of the 404.7 nm line (used as the comparison standard) yielded recorder indications for the ribbon lamp which were approximately 29 to 85 times greater than that produced by the excitation tube. It was reported that the ratio was much greater for the central region of the spectrum, but it became more favorable in the ultra-violet region. In the present work the standard lamp was situated approximately 2.7 meters from the entrance slit of the monochromator and a diaphragm was positioned at the standard lamp lens. In this manner the light intensity from the ribbon lamp was reduced to a level comparable to that observed for the principal transitions. The ratio of the recorder indications for the excitation tube and ribbon lamp fluctuated as a function of wavelength,

and were most favorable for the principal transitions of the Hg spectrum. The 404.7 nm line was characterized by a recorder indication for the excitation tube which was from 3 to 37 times larger than that of the ribbon lamp. Twelve measurements at ratios lying within the above limits, were averaged to yield a measurement which was repeatable to within 5.5%. The ratio of the respective recorder indications were more favorable for strong spectral lines which lie in the central region of the visible spectrum, (e.g. the 546.1 nm line yielded a recorder indication for the ribbon lamp which was from 1 to 6 times larger than that of the excitation tube). It must also be noted that the ratio of the recorder indications was much greater for extremely weak spectral lines.

An examination of Table IX shows that the measurements of the present work are consistently larger with the exception of the $6^3D_3 - 6^3P_2$ (365.0 nm) and $6^3D_1, 6^1D_2 - 6^3P_2$ (366.3 nm) transitions. One may speculate that the origin of these discrepancies, lies in part within the calibration techniques used in the two laboratories. The method employed by Jongerius has the advantage of simple optical relationships (e.g. the solid angle subtended by the collision chamber and ribbon lamp are identical), but it exhibits the major disadvantage of producing a consistently large ratio between the recorder indications corresponding to the ribbon lamp and excitation tube. Because of this the individual measurements are made under dissimilar operating conditions for the detection apparatus.

Intensity Ratios of Lines Originating from a Common Upper Level

The intensity of a spectral line is given by the expression

$$I = N(j) \frac{A(j,k)}{\lambda(j,k)} \cdot hc, \quad (29)$$

where $N(j)$ is the population of the upper level, $\lambda(j,k)$ is the wavelength of the radiation, emitted in the $j \rightarrow k$ transition, hc is a constant equal to 1.99×10^{-16} erg-cm, and $A(j,k)$ is the spontaneous transition probability. From the form of this expression it is evident that transitions emanating from a common upper level will have their intensities occurring in a ratio which is independent of the population of the upper level. This ratio is also related to the experimentally determined effective excitation cross sections through the relation

$$\frac{I'}{I} = \frac{Q(j,k) \lambda(j,m)}{Q(j,m) \lambda(j,k)}. \quad (30)$$

The theoretical and experimental intensity ratios have been determined for the visible mercury triplet, which has the 7^3S level common to all of the transitions. The results of this investigation are displayed, along with the experimental ratios reported by other investigators in Table X.

The ratios were shown to be independent of the incident electron energy by Ende ⁽³³⁾, therefore the results are presented at the energies reported by the authors. The more recent measurements of Jongerius and this paper exhibit a significant deviation from the predicted theoretical values. In contrast the experiments of the early 1930's yield ratios which are in general

TABLE X
INTENSITY RATIOS OF THE VISIBLE MERCURY TRIPLET

Investigator	$I(7^3S, 6^3P_2)$	$I(7^3S, 6^3P_1)$	$I(7^3S, 6^3P_0)$
Theory (this paper)	70	100	46
Experiment (this paper)	95 ± 13	100	35 ± 3
Jongorius	100	100	38
Thieme	72	100	40
Ende	60	100	49
Hanle and Schaffernicht	82	100	46

agreement with the theory. The early measurements were made employing photographic emulsions as detection devices. Because of the difficulties associated with their calibration one would question Ende's claim of 5% accuracy.

The present work investigated the mechanisms of self absorption of the emerging light by atoms in the 6^3P states, and stepwise excitation of atoms from these states, as possible factors which tended to distort the experimental ratio. The variation of light output as a function of pressure was observed to obey a linear relationship for the $7^3S - 6^3P_{2,1,0}$ transitions. In addition an estimate of the order of magnitude of the absorption coefficient yielded an extremely small value. The cross section for stepwise excitation from the 6^3P levels was estimated by Fabrikant to be of the order of 10^{-16} cm^2 for the case of high electron current densities. The occurrence of a stepwise process would be indicated by a quadratic dependence of the light output upon the electron beam density. No such dependence was found to exist for the electron current range used in the investigation. The absence of these perturbing effects seems to indicate that the origin of the discrepancy lies outside of the realm of experimental technique. However, the apparent disagreement between the theoretical and experimental ratios may be fortuitous. This possibility exists because the theoretical values were calculated under a single configuration approximation which ignores the existence of non-diagonal electrostatic and spin-other orbit interactions connecting different configurations. The inclusion of a configuration interaction term into the wave functions could lead to an

appreciably different ratio. At present no detailed calculation has been carried out to estimate the magnitude of this effect.

Further studies were also carried out for the intensity ratios of spectral lines emanating from the 7^1S and n^1P levels ($n = 8, 14$). The experimental values are compared to the theoretical intensity ratios and the results are displayed in Table XI.

One notes that the 7^1S and 8^1P levels are characterized by ratios which exhibit good agreement with the corresponding theoretical values. The remaining n^1P levels have ratios which show reasonable agreement, with the exception of the transitions originating from the 9^1P and 10^1P levels. However one should exhibit caution in forming definite conclusions concerning the apparent agreement between the experimental and theoretical ratios for large values of n . It is very probable that the high lying states experience a strong configuration interaction with neighboring states. This possibility is neglected in the theoretical model considered in this paper, therefore the theoretical ratios may not be a true representation of the line intensities.

TABLE XI

INTENSITY RATIOS OF LINES ORIGINATING FROM THE 7^1S AND n^1P LEVELS

Transition	Wavelength (nm)	Intensity Experiment	Ratio Theory	Mixing Coefficients (a^2/b^2)
$7^1S - 6^1P$ $7^1S - 6^3P_1$	1013.9 407.8	2.0	0.94	35.8
$8^1P - 7^1S$ $8^1P - 7^3S$	671.6 607.2	1.5	1.9	2.8
$9^1P - 7^1S$ $9^1P - 7^3S$	623.4 567.6	1.4	13.	19.
$10^1P - 7^1S$ $10^1P - 7^3S$	580.3 531.7	0.59	10.	12.
$11^1P - 7^1S$ $11^1P - 7^3S$	554.9 510.2	3.0	3.0	4.3
$12^1P - 7^1S$ $12^1P - 7^3S$	539.3 497.0	1.8	3.1	4.3
$13^1P - 7^1S$ $13^1P - 7^3S$	529.0 488.3	1.2	3.1	4.3
$14^1P - 7^1S$ $14^1P - 7^3S$	521.8 482.2	0.82	3.1	4.3

Note: The ratio of a^2/b^2 for the levels 11^1P , 12^1P , 13^1P and 14^1P was obtained from a theoretical estimate of the mixing coefficients. The values of a^2 and b^2 are estimated to be 0.81 and 0.19 respectively.

CHAPTER V

CASCADE ANALYSIS

The experimental investigation, discussed in this paper, was carried out under the conditions of low electron beam current and atom number density. Under these conditions the influence of superelastic collisions is negligible and for a steady state condition the decrease of population of the j th level, due to radiative transitions, is equal to its gain in population, due to cascade transitions from higher states and electron impact. The population rate equation is given as

$$A(j)N(j) = \sum_{i>j} N(i)A(i,j) + N(g) \left(\frac{I}{es}\right)Q(j) \quad (31)$$

where $N(i)$ and $N(j)$ are the respective number densities of the i th and j th states, $A(i,j)$ is the probability of a radiative transitions from the i th to the j th state and $A(j)$ denotes the total radiative transition probability for transitions from the j th level to all lower levels.

An expression for the direct excitation cross section in terms of

the empirical effective cross sections, and the theoretical branching ratio follows from equation (31). The direct cross section is given by the expression

$$Q(j) = Q'(j) - \sum_{i > j} Q(i, j), \quad (32)$$

where $Q'(j)$ is equal to the product $Q(j, k) B(j, k)$ and is defined as the apparent excitation cross section. The apparent cross section is uncorrected for the effects of cascade contributions. Therefore, in order to determine the direct cross section, the contributions of all levels lying above the j th state are subtracted from it. For the case of electron excitation of helium the contribution to the apparent cross section, from cascade transitions usually amounts to less than 15% of its total value. This criteria is not valid for some of the mercury levels which were studied in this work. One observes that the levels can be classified into two categories; (1) those levels which experience small population gains through cascade transitions and (2) levels whose major population mechanism is cascade from upper levels. States which typify each of these categories will be examined in the following sections.

Direct Excitation Cross Section, 6^3D_3 Level

The cross section for excitation to the 6^3D_3 state by electron impact is expressed as,

$$Q(6^3D_3) = Q'(6^3D_3) - \sum_{n \geq 8} Q(n^3P_2, 6^3D_3) \quad (33)$$

where the cascade contribution from the nF states ($n \geq 6$) is assumed to be

negligible. The apparent cross section, $Q'(6^3D_3)$, was experimentally determined at an electron energy of 15 eV, to be $(7.5 \pm 1.3) \times 10^{-18} \text{ cm}^2$. (In this case one notes immediately that the branching ratio is unity.) The contribution to its population by cascade transitions was estimated through the following relation,

$$Q(n^3P_2, 6^3D_3) = \frac{A(n^3P_2, 6^3D_3)}{A(n^3P_2, 7^3S)} \cdot Q(n^3P_2, 7^3S), \quad (34)$$

where $n = (8, 14)$. The transition probabilities were calculated by E. T. P. Lee using Slater type wave functions, and the effective cross sections of the $nP - 7^3S$ series are those reported in this work. The individual contributions of the n^3P_2 levels were summed to yield a value of $(2.2 \pm .5) \times 10^{-20} \text{ cm}^2$. This procedure indicates that the cascade contribution to the 6^3D_3 level is an extremely small fraction of the apparent cross section at an energy of 15 eV. Although this quantity is but an estimate of the true contribution, it indicates that the true value should not exceed a few percent of the total cross section. The direct cross section, at an incident electron energy of 15 eV, is determined as $(7.5 \pm 1.3) \times 10^{-18} \text{ cm}^2$.

Direct Excitation Cross Section, 6^3D_2 Level

In a manner similar to the previous case, one can express the direct cross section for the 6^3D_2 level by the equation,

$$Q(6^3D_2) = Q'(6^3D_2) - \sum_{n \geq 8} Q(nP, 6^3D_2). \quad (35)$$

The above expression assumes that the nF states contribute a negligible amount to the population of the 6^3D_2 level. The apparent cross section of the state is equal to the product of the effective excitation cross section, describing the $6^3D_2 - 6^1P$ transition, and the theoretical branching ratio. The effective cross section has a value of $(2.8 \pm .3) \times 10^{-18} \text{ cm}^2$ at an energy of 15 eV, while the branching ratio has the calculated value of 25 ± 7 (cf. Table II). Therefore the apparent cross section becomes $(7.0 \pm 2.) \times 10^{-17} \text{ cm}^2$. The 6^3D_2 level is a mixed state, possessing both singlet and triplet characteristics, therefore one would expect the contribution from cascade transitions to be larger than in the case of the 6^3D_3 state, which is a pure triplet state. The cascade contribution is estimated by employing a relationship similar to equation (34). However in this case transitions from the n^3P_1 and n^1P states are also possible, hence their contribution is included into the estimate. The individual contributions are summed and yield a value of $(3.8 \pm .9) \times 10^{-18} \text{ cm}^2$. In this case the cascade transitions account for approximately 6 percent of the total cross section. The total cross section is not greatly influenced by transitions from high lying levels, therefore one would expect its value to be a nearly true representation of the collision process. However, one must note that its magnitude is dependent upon the values of the singlet-triplet mixing coefficients for the $(6s)(6p)$ and $(6s)(6d)$ configurations and therefore depends

upon the atomic model used in calculating these quantities. Therefore the direct cross section is estimated as $(6.6 \pm 2.) \times 10^{-17} \text{ cm}^2$.

Direct Excitation Cross Section, 7^3P_2 Level

The spectral transitions, originating from the 7^3P_2 level have wave lengths which lie in the near infra-red region of the spectrum. The low intensities of the lines prohibits the use of conventional photomultiplier tubes or solid state devices as detectors. Fortunately the $7^3P_2 - 7^3S$ (1128.7 nm) transition lies within the sensitivity of a hypersensitized photographic emulsion, and can be observed after a relatively long exposure (e.g. 5 hours for the normal operating conditions of the excitation tube). However, the order of magnitude of the direct cross section to the 7^3P_2 state can be obtained from transitions lying in the visible region, by analyzing the cascade contribution to the 7^3S level. One expresses the direct cross section for the 7^3S level in terms of its apparent cross section and the cascade contributions as

$$Q(7^3S) = Q^*(7^3S) - \sum_{n \geq 7} Q(nP, 7^3S). \quad (36)$$

The apparent cross section is determined by the product of the effective cross section for the $7^3S - 6^3P_1$ transition and the appropriate branching ratio. This former quantity is equal to $(1.4 \pm .2) \times 10^{-17} \text{ cm}^2$ at an electron energy of 15 eV. The effective excitation cross sections listed in Tables IV and V were used to obtain the cascade contribution from the nP levels ($n = 8, 14$). Their sum yielded a value of $(2.1 \pm .3) \times 10^{-18} \text{ cm}^2$ as the total contribution from all

possible transitions. Contributions from states with $n \geq 14$ were estimated by extrapolation of the available experimental data. It was observed that the cross sections for levels with large values of n , ($n \geq 11$), followed the relation An^{-q} , where q was determined as approximately 3. The quantity A represents a constant which is determined by fitting the experimental values to the analytic expression. The summation of cross sections is replaced by an integral of the analytic expression which is evaluated within the limits $n = 14$ to $n = \infty$. Its evaluation yields an estimate of $2. \times 10^{-19} \text{ cm}^2$ for the cascade contribution of the higher levels.

In addition, one observes that the cross sections corresponding to levels with low values of quantum number n , experience a rapid increase for decreasing values of n . Therefore extrapolation of the experimental data to small values of n requires that all of the available data be used to obtain a "best fit" graphical approximation. The criteria for the selection of an extrapolated value will be the "best fit" approximation.

The $7P$ levels are the dominant cascade contributors, therefore their contribution is isolated from the remainder. The transitions involving these levels lie beyond the sensitivity of the detectors used in this work. Therefore, an estimate of their contribution to the population of the 7^3S level, through cascade transitions, is obtained from an extrapolation of the experimental data. One obtains an estimate of the effective cross section for the $7^3P_1 - 7^3S$ transition through extrapolation of the experimental

values $Q(n^3P_1, 7^3S)$. This procedure yields a value of $7.2 \times 10^{-19} \text{ cm}^2$ for the cascade contribution of the 7^3P_1 level, at an electron energy of 15 eV. In a similar manner the cascade contribution of the 7^1P level is estimated from the extrapolation of the experimental values $Q(n^1P, 7^3S)$. The effective cross section, $Q(7^1P, 7^3S)$, is estimated as $9.6 \times 10^{-19} \text{ cm}^2$.

The effective cross sections obtained by direct experimental measurements and extrapolation of the measured values are substituted into equation (36). The expression for the 7^3S direct excitation cross section then assumes the form

$$Q(7^3S) + Q(7^3P_2, 7^3S) + Q(7^3P_0, 7^3S) = 1.0 \times 10^{-17} \text{ cm}^2 \quad (37)$$

However, one notes that the branching ratios for the 7^3P_2 and 7^3P_0 states are unity. Therefore, the effective cross sections are equal to the corresponding apparent cross sections and equation (37) becomes

$$Q(7^3S) + Q'(7^3P_2) + Q'(7^3P_0) = 1.0 \times 10^{-17} \text{ cm}^2. \quad (38)$$

If the cascade contributions to the 7^3P_2 and 7^3P_0 levels are small, their apparent cross sections are approximately equal to the corresponding direct cross sections. Therefore one examines the cascade contributions, to insure that they are negligible.

The 8^3S level is the major cascade contributor to the population of the 7^3P_2 level therefore one investigates the magnitude of its contribution.

To obtain an upper limit of its influence one examines the relation

$$Q(8^3S) = Q(8^3S, 7^3P_2) - B(8^3S, 7^3P_2) - \sum_{n \geq 8} Q(n^3P, 8^3S) \quad (39)$$

which describes the mechanisms which populate the upper level. The direct cross section of the 8^3S level is less than that of the 7^3S level, therefore one places an upper limit of 10^{-17} cm^2 upon this value, ($Q(7^3S)$ calculated by Lee yields a value of $5 \times 10^{-19} \text{ cm}^2$ at 15 eV). In addition one would expect the affect of cascade transitions into the 8^3S level to be less than that for the 7^3S level. Thus one obtains as its upper limit the value,

$$\sum_{n \geq 8} Q(nP, 8^3S) \leq 2.2 \times 10^{-18} \text{ cm}^2. \quad (40)$$

The branching ratio for the $8^3S - 7^3P_2$ transition has the calculated value 6×10^{-3} , therefore one obtains an estimate of $4 \times 10^{-21} \text{ cm}^2$ for the 8^3S cascade contribution. This quantity is extremely small and will make up only a small percentage of the total cross section. The 6^3D_2 level has optically allowed transitions between both the 7^3P_2 and 6^3P_2 levels. The value of the cross section of the $6^3D_2 - 7^3P_2$ transition is estimated through the relation

$$Q(6^3D_2, 7^3P_2) = \frac{A(6^3D_2, 7^3P_2)}{A(6^3D_2, 6^3P_2)} \cdot Q(6^3D_2, 6^3P_2), \quad (41)$$

where $Q(6^3D_2, 6^3P_2)$ is of the order of 10^{-18} cm^2 at 15 eV. Meanwhile the ratio of the transition probabilities is determined as approximately 2×10^{-7} , which leads to an extremely small value for the desired cross section. Even though this analysis leads to a rough approximation of the true value, one observes that the cascade contribution is negligibly small. This analysis can be extended to the other members of the 7P levels with similar results. Therefore one justifies the use of the approximation $Q(7^3P) \simeq Q(7^3P)$ in equation (38).

Previous experimental evidence indicates that the 7^3S direct cross section will be small, as compared to that of the 7^3P states. This claim is also supported by theoretical calculations which predict $Q(7^3P) \approx 100 Q(7^3S)$ at an electron energy of 15 eV. Therefore equation (38) becomes

$$Q(7^3P_2) + Q(7^3P_0) \approx 1. \times 10^{-17} \text{ cm}^2 \quad (42)$$

The theoretical calculations of Lee show that the 7^3P_0 cross section is approximately one-tenth of the 7^3P_2 value, therefore the direct cross section of the 7^3P_2 level can be estimated as $1 \times 10^{-17} \text{ cm}^2$, at an electron energy of 15 eV.

A later direct measurement of the $7^3P_2 - 7^3S$ effective cross section yielded a value of $(2.5 \pm .8) \times 10^{-17} \text{ cm}^2$, for incident electrons of 15 eV energy. The branching ratio for this transition is unity, and, as was shown previously, the population of the 7^3P_2 level is not greatly influenced by cascade transitions. Because of this, one can estimate a value of $(2.5 \pm .8) \times 10^{-17} \text{ cm}^2$ for the direct excitation cross section. This value exhibits reasonable agreement with the value obtained from the examination of the 7^3S

population mechanisms. Hence, this type of analysis provides a means by which a previously unattainable cross section can be estimated.

Direct Excitation Cross Section; 7^1S Level

As in the three previous cases the direct cross section of a particular level can be expressed as the difference between its apparent cross section and the cascade contributions into the level. For the 7^1S level this relationship is expressed by the equation

$$Q(7^1S) = Q'(7^1S) - \sum_{n \geq 7} Q(nP, 7^1S). \quad (43)$$

The contribution to the total cross section from the n^1P levels was obtained through experimental measurements and extrapolation of these measurements. The contribution of the n^1P levels ($n = 8, 14$) was measured as $1.8 \times 10^{-18} \text{ cm}^2$. The effective cross sections of the $n^1P - 7^1S$ transitions with $n = 10, 14$ were observed to obey the analytic expression An^{-q} where q is approximately equal to 4.5. Integration of this analytic expression yielded a value of $6 \times 10^{-20} \text{ cm}^2$ for the contributions from levels with a principal quantum number greater than 14. The value of the $7^1P - 7^1S$ effective cross section was obtained through extrapolation of the experimental measurements, and yielded a value of $2.0 \times 10^{-18} \text{ cm}^2$ at 15 eV. No intercombination transitions were observed, therefore the contribution of the 7^3P_1 level was estimated from knowledge of the quantity $Q(7^3P_1, 7^3S)$ and the relation

$$Q(7^3P_1, 7^1S) = Q(7^3P_1, 7^3S) A(7^3P_1, 7^1S)/A(7^3P_1, 7^3S) . \quad (44)$$

Extrapolation of the experimental data yields $Q(7^3P_1, 7^3S) = 7.2 \times 10^{-19} \text{ cm}^2$

while the ratio of the transition probabilities was determined to be 0.24 (cf.

Table II). This procedure yielded a value of $1.7 \times 10^{-19} \text{ cm}^2$ at an incident electron energy of 15 eV. Since the 7^3P_1 is the major contribution of the intercombination series, it is assumed that the remaining levels will contribute a negligible amount. The individual contributions were summed to give the equation

$$Q(7^1S) = Q'(7^1S) - (4.0 \pm .8) \times 10^{-18} \text{ cm}^2. \quad (45)$$

Effective excitation cross sections were observed for two transitions involving the 7^1S level as the upper state. The intercombination transition at 407.8 nm and the normal transition occurring at 1013.9 nm. The latter transition was observed by means of a hypersensitized photographic plate, and yielded a value of $(6.4 \pm 1.3) \times 10^{-18} \text{ cm}^2$ at 15 eV. The cross section of the $7^1S - 6^3P_1$ intercombination transition, was measured at 15 eV and determined to be $(1.3 \pm .2) \times 10^{-18} \text{ cm}^2$. The magnitude of the apparent cross section is directly dependent upon the value of the theoretical branching ratio and therefore upon the values of the singlet-triplet mixing coefficients. The value of the branching ratio is very sensitive to the magnitude of the coefficients, and especially so for the intercombination transition. This can be illustrated by calculating the cross section for values of the mixing coefficients determined by different means. From fine structure calculations (cf. Chapter ii) one can obtain values of a and b which lie in the range 0.978 to 0.993 and 0.21 to 0.120 respectively. The smallest value of b would yield

a branching ratio for the intercombination transition, of 5.5 and an apparent cross section of $7.2 \times 10^{-18} \text{ cm}^2$. However, if one chooses to use the intermediate values $a = 0.98$ and $b = 0.169$ which are the average of the values obtained from separate experimental and theoretical quantities, then the branching ratio decreases to 3.1 and the apparent cross section becomes approximately $4 \times 10^{-18} \text{ cm}^2$. Therefore the magnitude would be extremely sensitive to the choice of mixing coefficients and vary from approximately zero to $3.2 \times 10^{-18} \text{ cm}^2$. If one uses the apparent cross section obtained from the $7^1\text{S} - 6^1\text{P}$ transition, the analysis yields a result which is less sensitive to the value of the mixing coefficients. Using the mixing coefficients described above, one obtains values of 1.22 and 1.45 for the respective branching ratios. This leads to apparent cross sections which lie within the range $(7.8 - 9.3) \times 10^{-18} \text{ cm}^2$. Hence the direct cross section will possess a value within the range $(3.8 - 5.3) \times 10^{-18} \text{ cm}^2$. Observation of the normal transition yields a better indication of the direct cross section than that provided by the intercombination line. In either case the cascade contribution comprises an extremely large part of the total cross section.

Comparison With Theory

Estimates of the direct excitation cross sections for four excited states of mercury were obtained through an analysis of the cascade contributions to these levels. Theoretical calculations of the direct cross sections

were carried out by E. T. P. Lee at the University of Oklahoma. The calculations were made employing the Born and Born-Oppenheimer approximations for the case of inelastic electron-atom scattering. The results obtained by Lee are displayed in Table XII, along with the experimental values obtained in the previous section. The theoretical and experimental values exhibited good agreement for the states which were not affected by singlet-triplet mixing (e.g. the 7^3P_2 and 6^3D_3 levels). However, a significant difference exists between the theoretical and experimental values for the 6^3D_2 level. It is believed that the discrepancy can be traced directly to the uncertainty present in the mixing coefficients. The direct cross section was calculated through the observation of the $6^3D_2 - 6^1P$ intercombination transition. Since both states exhibit singlet-triplet mixing the branching ratio is dependent upon four such coefficients, each of which possess a range of acceptable values.

The largest discrepancy between the theoretical and experimental values occurs for the cross section of the 7^1S state. The theoretical calculation yields a value which is nearly 30 times larger than the corresponding experimental value. The present value of the effective cross section of the $7^1S - 6^3P_1$ transition is in general agreement with the value reported by Jongerius. In addition the ratio of the line intensities, corresponding to the $7^1S - 6^1P$ and $7^1S - 6^3P_1$ transitions, is in good agreement with that predicted by theory. Also it is highly unlikely that the measurements of this cross section could experience such a gross error due to experimental inaccuracies. There-

fore, the origin of this discrepancy must lie outside the realm of experimental mis-measurement. One does note, however, that cascade transitions constitute a major portion of the total cross section, and that the value of the apparent cross section is very sensitive to the magnitude of the mixing coefficients. Even with these considerations in mind, one cannot justify such a large discrepancy with the information now available.

TABLE XII
COMPARISON OF EXPERIMENTAL AND THEORETICAL
DIRECT EXCITATION CROSS SECTIONS

Incident electron energy 15 eV.

Level	Theory (10^{-18} cm^2)	Experiment (10^{-18} cm^2)
6^3D_3	8.8	7.5
6^3D_2	18	66
7^3P_2	37	25
7^1S	110	4

CHAPTER VI

CONCLUSIONS

Optical excitation functions for 40 transitions of the mercury spectrum were obtained, under conditions of low pressure and low electron beam current. Because of the complex nature of the spectrum, only 30 percent of the transitions were completely resolved from neighboring lines of the Hg I and Hg II spectrum. The failure to experience adequate spectral resolution caused the shapes of many of the weaker lines to be distorted. Thus it was difficult to form definite conclusions concerning the general shapes of the curves. Nevertheless it was possible to conclude that the triplet levels are usually characterized by sharp maxima near their onset and experience a rapid decline thereafter. The $1p$ levels are characterized by curves which possess a shallow peak near their onset and rise to broad maxima at approximately 30 eV. One notes a similarity in shape between the above mentioned curves and those obtained for the excited states of helium. The $1s$ levels are characterized by curves which are unique in that they possess steep peaks near their onset and broad maxima, of comparable height, occurring at approximately

30 eV. The initial peaks may be attributed to the population of the $1S$ levels through intercombination transitions from higher $3p$ states, while the broad maxima are characteristic of the direct excitation of the singlet levels by electron impact. Much of the fine structure, which appears in the various excitation functions, can be similarly attributed to the population of the levels by cascade transitions. The shapes of the excitation functions are in good agreement with those obtained by other investigators, employing apparatus of similar design.

Absolute measurements of the effective excitation cross sections yielded values which were constantly larger, for the visible portion of the spectrum, than those reported by Jongerius. It is speculated that the discrepancy has its origin in the calibration techniques employed in the two laboratories. The measurements of the $7^3S - 6^3P_{2,1,0}$ cross sections were used to investigate the experimental intensity ratios of the visible triplet. These ratios were compared to the theoretical ratios and a significant discrepancy was noted. The disagreement was due in part to the inadequacy of the single configuration approximation used to calculate the theoretical values.

In addition, the effective cross section measurements were used, in conjunction with the theoretical branching ratios to obtain estimates of the direct excitation cross sections of the 6^3D_3 , 6^3D_2 , 7^3P_2 , and 7^1S states. The $3D$ and $3p$ states are not affected to a large extent by the influence of cascade transitions, which constitute but a few percent of the total cross section. The

6^3D_3 and 7^3P_2 cross sections exhibit good agreement with the theoretical values at an incident electron energy of 15 eV.

The direct cross section of the 6^3D_3 state was obtained through the observation of the $6^3D_3 - 6^3P_2$ transition. Neither level experiences singlet-triplet mixing, therefore the branching ratio is free from inaccuracies introduced by the range of values of the mixing coefficients. The experimental value of $7.5 \times 10^{-18} \text{ cm}^2$ exhibits good agreement with the theoretical value of $8.8 \times 10^{-18} \text{ cm}^2$ at an electron energy of 15 eV.

The 6^3D_2 level is characterized by an experimental cross of $66 \times 10^{-18} \text{ cm}^2$ which is approximately 3 times larger than the corresponding theoretical value. The disagreement is partly attributed to the range in the magnitude of the $(6s)(6d)$ and $(6s)(6p)$ mixing coefficients, which are used in the calculation of the theoretical branching ratio. It is possible to reduce the range of the values by restricting the experimental observations to non-intercombination transitions.

An analysis of the cascade contributions to the 7^3S level showed that cascade transitions dominated the true value of the 7^3S direct cross section. This apparent liability allowed one to obtain an order of magnitude estimate of the direct cross section for excitation to the 7^3P_2 level. The estimate of $1 \times 10^{-17} \text{ cm}^2$ compared favorably to the actual cross section, which was later determined as $(2.5 \pm .8) \times 10^{-17} \text{ cm}^2$ at 15 eV. The latter value exhibited good agreement with the theoretical value of $3.7 \times 10^{-17} \text{ cm}^2$.

Contributions to the population of the 7^1S level by cascade transitions constituted a major portion of the total cross section. The range of acceptable values of the $(6s)(6p)$ mixing coefficients resulted in a large uncertainty in the direct cross section obtained from the observation of the intercombination transition. The direct cross section obtained from observation of the intercombination transition varied from zero to $3.2 \times 10^{-18} \text{ cm}^2$ at an energy of 15 eV. The limits of the variation were reduced by basing the calculation of the direct cross section upon the absolute measurement of the $7^1S - 6^1P$ effective cross section. This procedure yielded an estimate of the direct cross section which varied from $3.8 \times 10^{-18} \text{ cm}^2$ to $5.3 \times 10^{-18} \text{ cm}^2$ at 15 eV. Nevertheless this value was observed to be approximately 30 times smaller than the corresponding theoretical prediction. It is believed that the origin of this discrepancy does not lie within the experimental measurements, but instead is due to theoretical uncertainties present in the determination of the branching ratio and the direct cross section.

Because of the uncertainties introduced by the range of acceptable values for the mixing coefficients, it is evident that valid estimates of the direct excitation cross sections can be best obtained through observation of non-intercombination transitions.

LIST OF REFERENCES

1. White, D., Phys. Rev. 28, 1125 (1926)
2. Bricout, P., J. Phys. Radium 9, 88 (1927)
3. Orstein, L. S., Z. Physik 83, 171 (1933)
4. Smit, J. A., and H. M. Jongerius, Appli. sci. Res. B5, 59 (1956)
5. Bogdanova, I., Bull. Acad. Sci., USSR Phys. Ser. Engl. Trans. 27, 1029 (1963)
6. Jongerius, H. M., Measurements of Optical Excitation Functions of the Mercury Atom, (Excitation by Electrons) (Dissertation, 1961, University of Utrecht)
7. Lee, E. T. P., University of Oklahoma, Unpublished Data
8. National Bureau of Standards, Circular 467 Vol. III 1958
9. Lurio, A., Phys. Rev. 140, A1505 (1965)
10. Semenov, R. I. and B. A. Strugach, Opt. and Spectr. 18, 428 (1965)
11. Wolfe, H., Phys. Rev. 41, 443 (1932)
12. VanKleef, Th. A. M. and M. Fred, Physica 29, 389 (1963)
13. Condon, E. U. and Shortley, G. H. The Theory of Atomic Spectra (Cam-

bridge University Press, Cambridge, 1959), chap. III

14. Mishra, B., Proc. Camb. Phil. Soc. 48, 511 (1952)
15. Ernsberger, F. M., and H. W. Pitman, Rev. sci. Inst. 26, 584 (1955)
16. Frisch, S., Spectrochim. Acta 11, 350 (1957)
17. Zapesochny, I. P., Leningr. Univ. Vestn. 9, 67 (1954)
18. Fabrikant, V., C. R. (Doklady) URSS 16, 263 (1937)
19. Schaffernicht, W., Z. Physik 62, 106 (1930)
20. Frisch, loc. cit.
21. Zapesochny, I. P., IV Int. Conf. on the Physics of Electronic & Atomic Collisions (Science Bookcrafters, Inc., Hastings, N.Y. 1965)
22. Thieme, O., Z. Physik 78, 412 (1932)
23. Schaffernicht, loc. cit.
24. Schaffernicht, ibid.
25. Zapesochny, loc. cit.
26. Frisch, loc. cit.
27. Jongerius, loc. cit.
28. Larabee, R. D., J. Opt. Soc. Amer. 49, 619 (1959)
29. DeVos, J. C., Physica 20, 715 (1954).
30. Hanle, W., and W. Schaffernicht, Ann. Physik 6, 905 (1930)
31. Fischer, O., Z. Physik 56, 503 (1929)
32. Miller, F. L., Excitation of Helium Atoms by Electron Impact (Dissertation, 1964, University of Oklahoma.

33. Ende, W., Z. Physik 56, 503 (1929)